CONF-8609126--5

THE JET IMPINGEMENT PHASE OF MOLTEN CORE-CONCRETE INTERACTIONS

J. J. Sienicki and B. W. Spencer*

CONF-8609126--5

DE87 004713

ABSTRACT

Scoping calculations have been carried out demonstrating that a significant and abrupt reduction in the corium temperature may be realized when molten corium drains as a jet from a localized breach in the RPV lower head to impinge upon the concrete basemat. The temperature decrease may range from a value of ~ 170 K (~ 140 K) for limestone (basaltic) aggregate concrete to a value approaching the initial corium superheat depending upon whether the forced convection impingement heat flux is assumed to be controlled by either thermal conduction across a slag film layer or the temperature boundary condition represented by a corium crust. The magnitude of the temperature reduction remains significant as the initial corium temperature, impinging corium mass, and initial localized breach size are varied over their range of potential values.

INTRODUCTION

For LWR severe accident sequences in which it is postulated that the reactor pressure vessel (RPV) lower head is breached in a localized manner, a jet of molten corium will flow from the breach to impinge upon the concrete basemat. Previous assessments of the ensuing Molten Core-Concrete Interaction (MCCI) phenomena have traditionally assumed that the corium melt is instantaneously formed as a layer atop the concrete and have not treated several potentially significant processes taking place during the initial impingement phase.

For low pressure sequences, the corium impinges normally upon concrete, flows radially over the cavity or pedestal floor, impinges on the surrounding walls, and accumulates as a layer upon the basemat. Upon contacting concrete, corium is expected to freeze to form a crust layer with molten corium flowing over crust as it spreads on the base. Concrete will begin to rapidly decompose and melt beneath the crust.

*Reactor Analysis and Safety Division, Argonne National Laboratory, Argonne, Illinois 60439.

The presence of the crust may be envisioned to present a temperature boundary condition for forced convection heat transfer but lacks sufficient strength to prevent the entrainment and mixing of the concrete melt products into the corium. A layer of melted concrete slag may be envisioned to exist interstitial to the corium and the remaining underlying solid concrete. However, gas liberated by the heatup and decomposition of the concrete passing through the slag layer may entrain molten slag into the overlying corium thereby limiting the thickness of the insulating slag film. Two processes principally contribute to a reduction in the corium temperature during the impingement phase. The first is the forced convection heat flux from the impinging and radially spreading corium stream into the underlying concrete. The second is the heat sink effect of decomposed and melted concrete entrained into the corium. In the vicinity of the corium jet impinging upon the concrete, extremely large forced convection heat transfer rates may be predicted far surpassing those encountered in traditional MCCI investigations.

A series of scoping calculations has been carried out to investigate the importance of the impingement phase heat transfer processes. The principal objectives are to estimate the reduction in the corium temperature as well as the extent of concrete erosion occurring during the impingement stage. A model was developed to predict the time dependent erosion of the concrete basemat by an impinging stream of corium liquid when a corium pool residing inside the RPV lower head drains through a breach. The existence or nonexistence of either a protective corium crust or a molten concrete slag layer at the corium-concrete interface in the presence of gas evolution are unknown at the present time. To encompass uncertainties in the corium-to-concrete heat transfer, calculations were therefore carried out alternately assuming the presence and absence of crust formation as well as the presence and absence of a slag film layer. Calculations were performed for both generic limestone and basaltic concrete types. The dependency of the corium temperature reduction and the concrete mass eroded upon the initial corium temperature, the total corium mass draining from the RPV, and the initial breach diameter were examined parametrically. The present study exclusively considers low pressure sequences for which the corium drains under gravity head and remains largely inside the cavity or pedestal region. For corium ejection at elevated RPV pressure, the phenomena involved in the interaction of corium with concrete could differ significantly from those discussed herein.

CALCULATIONAL MODEL

The erosion of the concrete basemat is closely related to the size of the RPV breach through which the corium is draining. As corium flows through the breach, ablation of the surrounding steel vessel wall will increase the breach size and hence the di-

ameter of the corium stream impinging upon the concrete. The time dependent velocity of corium flowing through the breach is given in terms of the decreasing gravity head of the corium pool remaining inside the RPV lower head. The ablation-induced growth of the circular vessel breach is predicted using a modified version of the wall ablation model discussed in Ref. 1. Two major assumptions form the basis of the vessel wall erosion analysis. First, melted vessel steel is assumed to flow downward as a thin film between the corium and the surrounding solid steel substrate. Second, the calculations assume that the corium oxide phase nominally freezes into thin pieces of crust interstitial to the flowing molten corium and the vessel steel melt film. The crust segments are envisioned to be swept along over the melt film tending to insulate the film and remaining solid steel from the hot molten corium. The corium mixture is assumed to consist of immiscible oxidic and metallic phases which are locally segregated such that short slugs of pure oxide and pure metal alternately flow through the vessel breach. Although the corium oxidic and metallic phases are locally segregated, the duration of flow of individual slugs of metal is assumed to be sufficiently short that an oxide crust may be assumed present at all times. It has been shown in Ref. 1 that wall erosion commences within at most several tenths of a second following the inception of corium flow. Accordingly, the short interval corresponding to the premelting heatup of the wall is ignored in the current calculations. Wall ablation is modeled as a quasi-steady process in which the erosion rate is defined in terms of the forced convection heat flux from the flowing corium and the change in the specific enthalpy of the vessel steel in going from its initial temperature to its final temperature in the molten state.

After the corium stream exits the breach, it accelerates under gravity and contracts in diameter. During its fall to the basemat, the corium stream will undergo a decrease in temperature as a result principally of thermal radiation from its periphery. Assuming that the heat loss is due exclusively to radiation from the circumference of the contracting jet, the bulk temperature of the corium at impingement is given by

$$T_i = \left\{ \frac{1}{T_b^3} + \frac{12\varepsilon S}{\rho_i C_i D_b} \frac{2}{3g} \left[\left(\frac{U_i}{U_b} \right)^{3/2} - 1 \right] \right\}^{1/3} . \qquad (1)$$

The high heat transfer rates resulting from impingement of the corium stream upon the concrete will result in the evolution of large quantities of gas due to concrete heating and decomposition. The gas initially rising from the concrete upper surface

will consist of steam resulting from the vaporization of both chemically bound and free water as well as CO_2 from decomposition of the carbonaceous constituents. If concrete ablation were not accompanied by gas evolution, then it might be expected that melted concrete slag would flow radially outward as a thin film between the impinging corium and the underlying solid concrete. Corium impingement heat transfer would also be expected to involve the formation of oxide crust segments interstitial to the flowing molten corium and the concrete slag film. When thermally stable, the crust segments would be expected to be dragged radially outward atop the molten slag film. Due to the large density ratio between the overlying corium and the concrete, the slag would be expected to buoyantly rise up into the accumulated corium pool beyond some distance from the jet centerline. The effects upon the concrete slag and corium crusts of the high gas flowrates resulting from concrete heating and decomposition have not yet been modeled. In view of the uncertainties involved, the concrete erosion rate is presently scoped with calculations making different assumptions about the existence or nonexistence of a concrete slag film and a corium crust layer. In particular, concrete ablation is alternately predicted for three sets of assumptions concerning the presence and absence of crust and slag film:

1. An oxide crust is assumed to be present when thermally stable and a molten film of concrete slag is assumed to exist between the corium and underlying solid concrete.

2. A concrete slag film is assumed to exist between the corium and underlying solid concrete but gas evolution is assumed to disrupt any oxide crust which may be present such that the crust effectively has no influence upon the heat transfer.

3. A corium crust is assumed invariably present between the flowing molten corium and the concrete but gas evolution is assumed to disrupt the concrete slag film such that the film effectively has no effect upon the heat transfer.

Heat transfer correlations for jet impingement flow are usually presented in terms of Nusselt numbers averaged over circular discs. The actual local heat flux decreases with the radial distance from the jet centerline. It shall be assumed here that beyond a specified scaled radius (nondimensionalized by the impinging jet diameter), negligible erosion of the surrounding concrete occurs. Thus, concrete erosion is envisioned to take place only within a circular disc surrounding the impinging jet. However, the jet diameter will progressively increase with time as a result of the ablation of the vessel steel surrounding the breach such that the size of the concrete erosion disc will accordingly grow with time. Within the erosion disc, a single mean heat transfer coefficient corresponding to a mean corium thickness erosion rate is assumed. The time dependent concrete mass eroded is thus

$$M_c = \rho_c \frac{\pi}{4} \int_0^t \frac{dZ_c}{dt} D_c^2 dt \qquad (2)$$

where D_c is the time dependent erosion disc diameter. Within the erosion disc, the concrete thickness erosion rate is assumed to be given by the quasi-steady expression,

$$\frac{dZ_c}{dt} = \frac{Q_i}{\rho_c \left[\Delta e_{c,liquidus} + \frac{1}{2} C_c \left(T_{int} - T_{c,melt} \right) \right]} \qquad (3)$$

Owing to the assumed local segregation of the corium oxide and metal phases, the actual erosion rate is assumed to be a corium volume fraction weighted average of the individual erosions calculated for predominantly pure oxide and pure metal flow. For concrete ablation, a protective oxide crust may or may not be thermally stable (i.e., may or may not completely remelt following its formation) depending upon the thermal conditions at the interface between the corium and the molten concrete slag film. The formulation of the erosion zone heat flux, Q_i, is dependent upon whether or not a crust exists. In the presence of crust formation, $Q_i = h_{conv} (T_i - T_{oxide,freeze})$. When crust formation does not occur, then $Q_i = h_{conv} (T_i - T_{int})$, where T_{int} is the temperature at the corium-slag film interface.

When a slag film is assumed to exist, a linear temperature profile is assumed across the film and an approximate expression is employed to estimate the slag film thickness. The film thickness is derived from consideration of laminar flow within the film, mass conservation between the film flow and the eroding basemat, a variable and temperature dependent viscosity across the thickness of the film, and equality of the shear stress within the film at its upper surface and within the molten corium at the bottom of the impingement flow boundary layer. The film thickness may be shown to be independent of the radius inside the impingement region.

The largest diameter disc for which circular jet impingement data are presented in Ref. 2 is equal to twenty times that of the impinging jet. Since the calculation totally ignores the heat transfer and ablation taking place outside of the idealized erosion disc, this value was selected for the erosion disc diameter in the present investigation to preclude an underestimate of the extent of concrete erosion. The forced convection heat transfer coefficient, h_{conv}, is accordingly taken equal to the disc averaged value recommended by Martin (2) for a disc of diameter, $D_c = 20\ D_j$, twenty times that of the impinging jet. It has been found convenient to fit the

function $Nu = 0.00187\ Re^{0.948}\ Pr^{0.42}$ to the Nusselt number values presented graphically in Ref. 2.

RESULTS

The concrete ablation heat transfer model was applied to the case of a corium stream draining from a single localized breach in a reactor system of Zion dimensions. For definiteness, the breach is assumed formed by the failure of a single instrumentation guide tube penetration weld resulting in ejection of the tube. The initial breach diameter is thus taken equal to 3.97 cm corresponding to the size of a single bored instrument guide tube penetration. The vessel wall is 13.7 cm thick and the corium is assumed to fall a distance of 4.93 m from the RPV to the basemat. The corium is assumed to have the composition 65.3 wt % UO_2, 10.8 wt % ZrO_2, 8.0 wt % Zr, 1.35 wt % Fe, 1.6 wt % Cr, and 0.8 wt % Ni in which half of the zircaloy cladding has undergone in-vessel oxidation. This composition is identical to that specified in the Nuclear Regulatory Commission Containment Loads Working Group PWR Standard Problem No. 1 for the investigation of containment loading following vessel failure (3). The U-Zr-O ternary phase is a sub-stochiometric oxide which begins to freeze at 2673 K (liquidus temperature). The Fe-Cr-Ni metal phase has a lower freezing temperature of 1767 K. A reference value for the corium mass ejected from the RPV of 86400 kg corresponding to roughly half the core inventory of fuel and the associated partially oxidized zircaloy cladding together with the below-core steel support structure shall be used in the discussion below. Similarly, an initial reference corium temperature of 2830 K, corresponding to 157 K of molten "superheat" or excess temperature above the oxide phase freezing temperature shall be assumed. The vessel wall is assumed to consist of Type A-533 steel. Calculations were performed for both limestone aggregate-common sand concrete and basaltic aggregate concrete having generic compositions similar to the default values specified in Ref. 4. In particular, the proportions of limestone aggregate-common sand concrete following decomposition are assumed to be 31.3 wt % CaO, 1.9 wt % MgO, 35.8 wt % SiO_2, 3.6 wt % Al_2O_3, 1.3 wt % FeO, 0.2 wt % TiO_2, 21.2 wt % CO_2, 2.0 wt % bound water, and 2.7 wt % free water. The corresponding proportions for basaltic aggregate concrete are 8.8 wt % CaO, 13.8 wt % MgO, 54.8 wt % SiO_2, 8.3 wt % Al_2O_3, 5.8 wt % FeO, 1.1 wt % TiO_2, 1.5 wt % CO_2, 2.0 wt % bound water, and 3.9 wt % free water. The concrete melting temperature (1670 K for limestone and 1650 K for basaltic) is taken equal to the concrete bulk liquidus temperature presented in Ref. 4. The formulations discussed in Ref. 4 were also used to obtain the temperature dependent molten slag viscosity and thermal conductivity.

Results obtained for limestone aggregate-common sand concrete shall be discussed first. For the reference value of superheat of 157 K, Fig. 1 shows as functions of

time the diameter of the RPV breach as well as the corresponding diameter of the accelerated and contracted corium stream impinging upon the basemat. Corium drains from the RPV over an interval of 127 s. During this time, the velocity of corium flowing through the breach decreases from 5.31 m/s to zero as the driving gravity head of the corium pool residing in the lower head continuously decreases. The corresponding velocity of the jet impinging upon the basemat varies from 11.2 to 9.84 m/s. The impinging jet is observed to have a maximum diameter of 13.4 cm. It is to be recalled that the concrete erosion disc is assumed to have a diameter twenty times that of the impinging jet such that the maximum erosion disc diameter is 2.68 m.

For ambient cavity pressures of 0.1 and 0.4 MPa, Figs. 2 and 3 respectively show the superficial velocity of gas rising through that portion of the corium pool above the erosion disc for the three different modeling approaches scoping the effects of the presence and absence of an oxide crust as well as a concrete slag film. For times beyond 22 s, the largest gas velocity is calculated for the case where the slag film is completely absent and the heat transfer is controlled by a crust. This reflects the prediction of higher heat fluxes in the absence of a slag film. The lowest gas evolution rates correspond to the case in which simultaneous crust formation and slag film growth are modeled. For this case, the oxide crust is actually predicted to be thermally stable only during the flow of the corium oxide phase and thermally unstable during the intermittent flow of the metal phase. For the 0.1 MPa pressure (representing a sequence in which steam arising from flashing of the primary system coolant has been condensed), the calculated superficial velocities range from 3.3 m/s when a crust and slag film are both present to 5.5 m/s when the film is absent and erosion is limited by an oxide crust. Raising the cavity pressure to 0.4 MPa (corresponding to sequences in which significant steam condensation has not taken place) increases the gas density and accordingly results in lower superficial velocities between 0.84 m/s (crust and slag film present) and 1.4 m/s (slag film absent). The gas fluxes are well in excess of those required for the formation of a churn turbulent flow regime (10 cm/s at 0.1 MPa and 5 cm/s at 0.4 MPa) (5). However, the gas velocities are an order of magnitude below those needed for the inception of a dispersed droplet flow regime (39 m/s at 0.1 MPa and 20 m/s at 0.4 MPa) (6). The pool void fraction above the erosion zone may be calculated from the superficial velocity using the correlation of Kataoka and Ishii (7) which predicts void fractions between 0.66 and 0.72 at 0.1 MPa and between 0.45 and 0.55 at 0.4 MPa.

Previous assessments of MCCI's have sometimes assumed that a stable and continuous gas film separates the overlying corium from the concrete analogous to a film boiling

regime. A possible criterion for the formation of a stable gas film is that the superficial gas velocity exceeds the threshold given by the results of Kutateladze and Malenkov (8) which under the present conditions provides

$$j = 30\left(\frac{\rho_g g}{P}\sqrt{\frac{\sigma}{g\Delta\rho}}\right)^{2/3}\left(\frac{\sigma g\Delta\rho}{\rho_g^2}\right)^{1/4} . \qquad (4)$$

For cavity pressures of 0.1 and 0.4 MPa, Eq. 4 predicts minimum superficial velocities of 3.3 and 1.7 m/s respectively which are comparable to those calculated to result from the impingement flow convective heat transfer rates. The current calculations thus indicate that the effects of the predicted high gas fluxes might result in blanketing of the concrete surface by a gas film which could preclude the intimate interfacial contact between corium and concrete assumed in the present analysis. The effects of potential gas film formation thus represent an additional uncertainty in the jet impingement phenomena.

Figure 4 shows the total mass of corium predicted to be ejected from the RPV versus time. The corium mass ejection rate increases with time principally due to the enlargement of the breach area corresponding to the slightly less than linear growth of the breach diameter (Fig. 1). The cumulative mass of concrete eroded for the three combinations of crust/film modeling assumptions is presented in Fig. 5. The increase in the erosion rate with time principally reflects the increase in the erosion disc diameter resulting from the growth of the breach diameter. The total ablated mass predicted when the impingement heat flux is limited by crust formation alone (i.e., gas evolution completely disrupts any slag film) is ~ 50% greater than that calculated assuming that heat transfer is limited solely by a slag film (gas generation disrupts the crust). For the case where a slag film is present without any crust, the effective driving ΔT for heat transfer is predicted to be less than the assumed superheat.

The temperature of the corium pool initially residing in the lower head at the time of vessel failure is dependent upon the progression of the in-vessel degradation and material relocation processes and is an area of uncertainty at the present time. To investigate the dependency of the impingement phase heat transfer phenomena upon the corium temperature, the superheat of the corium exiting the RPV breach was varied in a parametric fashion. The corium ejection/impingement time is seen to decrease from 234 to 76 s as the superheat is raised from 50 to 400 K (Fig. 6). For superheats below 50 K, it has been demonstrated previously (1) that the ejection times are long

enough that the potential for most of the corium to exit the vessel through a single localized breach may be exceeded by that for multiple localized failures or gross failure of the lower head steel thickness itself due to heatup-induced loss of strength. The dependency of the total concrete mass ablated upon the initial corium superheat is shown in Fig. 7. When the forced convection heat flux is controlled only by an oxide crust without any influence from a slag film, the total ablated mass increases slightly faster than linearly with the superheat. This approximately linear behavior is to be expected since the heat flux is directly proportional to the corium superheat. In contrast, when a slag film exists without any effects from crusting, the total eroded mass is much less sensitive to the superheat. Raising the superheat in this case results in a thicker slag film enhancing its thermal resistance and reducing the effective ΔT driving the forced convection heat transfer thereby tending to offset the effects of a higher corium temperature. When a slag film is assumed present but simultaneous crust formation is allowed, the crust is predicted not be be thermally stable at any time during impingement for superheats of ~ 300 K and above. As the superheat is progressively decreased below 300 K, oxide crust formation is thermally stable for a longer and longer portion of the impingement interval. For superheats below ~ 200 K, the crust is observed to significantly limit the total mass ablated, irrespective of the presence or absence of a slag film.

For each of the three sets of crust/film modeling approaches, Figs. 8-10 show as functions of the corium superheat the incremental reductions in the bulk temperature of the total impinged corium mass due to thermal radiation from the draining corium stream, forced convection from the corium as it flows through the impingement zone, and thermal equilibration of decomposed and melted concrete with the overlying corium. Also shown is the sum of these three contributions representing the total corium bulk temperature reduction. In the figures, the temperature decreases have been defined ignoring the heats of fusion of the corium oxide and metal phases such that temperature drops exceeding the initial superheat may be readily predicted. The temperature decrease arising from thermal radiation is seen to amount to only 14 to 16 K. The major contribution to the overall temperature reduction is that due to forced convection heat transfer from the corium stream as it impinges and spreads radially over the area of the erosion disc. Finally, thermal equilibration of the decomposed and melted concrete constituents with the corium provides an additional incremental temperature drop which may be as large as ~ 40% of that resulting from forced convection. Figure 11 compares the total temperature reductions predicted for the three sets of crust/slag modeling assumptions. Similar to the total eroded mass, the total temperature reduction limited by oxide crust formation in the absence of slag film effects increases slightly faster than linearly with the superheat. The

calculated total temperature reduction is observed to be larger than the value of the superheat indicating that the major portion of the superheat may be predicted to be lost during the impingement stage. At high superheats, the temperature reductions for the crust present-slag film absent case are significantly greater than those predicted assuming the existence of a nondisrupted slag film. For the case where a slag film is present without any crust formation, the total temperature decrease is not sensitive to the superheat. Total slag film controlled reductions vary only between 165 and 206 K over the range of superheats. For superheats below ~ 200 K, crust formation limits the temperature drop irrespective of the presence of a slag film. Thus, depending upon the presence or absence of either a protective crust or slag film, considerable uncertainty exists in the value of the corium temperature reduction which may be predicted during the impingement stage. The temperature decrease attained may range from ~ 165 K to a value representative of the major portion of the initial corium superheat.

Thus far, the calculations have assumed that a fixed total corium mass (86400 kg) impinges upon the basemat. For a fixed superheat of 157 K, the mass of the corium pool draining from the lower head was varied between 10000 and 138000 kg. The total corium bulk temperature reduction is observed to decrease as the ejected mass increases (Fig. 12). Raising the total corium mass results in ejection of a greater portion of the corium at larger breach diameters due to ablation-induced enlargement of the vessel breach. The decrease in the radiation heat loss from the draining corium stream and the decrease in the impingement heat transfer coefficient at larger jet diameters both contribute to lower temperature reductions upon impingement.

The initial localized breach size at the time of RPV failure may be both system and sequence dependent. For a PWR vessel without lower head penetrations, the results of Ref. 9 suggest that the initial hole diameter might be as large as 50 cm. For the reference conditions, Fig. 13 illustrates the dependency of the total corium temperature reduction upon the breach size. It is observed that significant temperature decreases of similar magnitude are predicted for initial hole diameters between 4 and 60 cm.

The calculations were repeated for basaltic aggregate concrete (Figs. 14-23). The lower gas evolution upon heatup and decomposition characteristic of basaltic concrete gives rise to lower superficial gas velocities relative to limestone concrete (Figs. 12 and 13 vs. 2 and 3). The gas velocities range from 1.5 to 3.4 m/s at 0.1 MPa and from 0.39 to 0.86 m/s at 0.4 MPa. The gas superficial velocities are thus predicted to border on or lie below the threshold for stable gas film formation

given by Eq. 4. The lower change in specific enthalpy in going from the initial temperature to the liquidus temperature for basaltic concrete means that for a fixed amount of energy deposited in solid concrete under quasi-steady conditions, a greater mass will be melted for basalt concrete than for limestone. For the case where the ablation heat flux is controlled by an oxide crust without any influence from a slag film, this characteristic combined with the higher specific heat of the basaltic decomposition products above melting generally results in the prediction of slightly larger temperature reductions for basaltic concrete relative to limestone. For example, assuming an invariably present crust, the temperature decreases due to thermal radiation from the draining corium stream and impingement zone forced convection are calculated to be identical for the two types of concrete. However, the larger mass ablated for basaltic concrete combined with the higher melted concrete specific heat results in a higher incremental temperature drop upon thermal equilibration. The total temperature drop limited by crust formation for basaltic is greater than that for limestone by a value ranging from 6 K at 50 K superheat to 53 K at 400 K superheat. These values are not large compared with the forced convection temperature reductions (31 K at 50 K superheat to 411 K at 400 K superheat) such that temperature decreases of similar magnitude may be expected for the two concrete types. On the other hand, for the case where the heat flux is strictly controlled by a slag film, the greater ablation potential of basaltic concrete gives rise to a thicker slag film which decreases the effective ΔT driving the forced convection heat losses thereby resulting in lower total temperature reductions relative to limestone. However, total temperature decreases of comparable magnitude are still calculated for the two variants of concrete.

DISCUSSION

Although the calculations have alternately assumed the presence and absence of an oxide crust or concrete slag film, the case in which the effects of both a crust and slag film are absent was not calculated. If gas evolution completely disrupts both the crust and slag film, then the effective ΔT driving the heat transfer may be of the order of 1000 K or more resulting in significantly greater concrete ablation and corium temperature reduction than presented here. Also, it should be noted that the predicted high gas evolution rates may enhance the "splashing" of corium onto other surfaces in the cavity thereby enhancing the corium quench as well as promote intermixing with any overlying water which might be present in the cavity.

CONCLUSIONS

In conclusion, scoping calculations have shown that processes during the impingement phase may significantly impact upon the MCCI phenomena ensuing immediately there-

after. It has been demonstrated that a significant and abrupt decrease in the corium temperature may be predicted due to the combined effects of impingement flow forced convection heat transfer and thermal equilibration of decomposed and melted concrete with the corium. The reduction in temperature will impact upon both the subsequent concrete attack as well as the release of fission products from the corium. The actual magnitude of the temperature reduction is subject to uncertainty because the basic physics involving the existence of either a crust of solidified oxide or a film of molten concrete slag at the corium-concrete interface are unknown in the presence of the indicated gas evolution rates. Moreover, an additional uncertainty involves the possible formation of a stable interstitial gas film separating corium from concrete as a result of the predicted large gas fluxes. For the assumed reference conditions of impinging corium mass and initial breach size, the temperature decrease may lie between ~ 170 K (~ 140 K) for limestone (basaltic) aggregate concrete and a value approaching the initial corium superheat depending upon whether the forced convection heat flux is controlled either by thermal conduction across a slag film layer or the temperature boundary condition represented by a corium crust. Temperature reductions of similar magnitude are predicted for both generic limestone and basaltic aggregate concrete types. The magnitude of the temperature decrease remains significant as the corium mass impinging upon the basemat as well as the size of the initial localized RPV breach are varied over the range of potential values. Resolution of the uncertainties in modeling the impingement phase phenomena would require well instrumented reactor material experiments in which molten corium jets are impinged upon prototypic concrete slabs combined with more detailed analysis of the test results.

NOMENCLATURE

C	=	specific heat, J/(kg•K)
D_b	=	diameter of corium jet exiting breach, m
D_c	=	diameter of concrete erosion disc, m
D_j	=	diameter of corium jet impinging upon concrete, m
$\frac{dZ_c}{dt}$	=	mean concrete thickness erosion rate within erosion disc, m/s
g	=	gravitational acceleration, m/s^2
h_{conv}	=	mean forced convection heat transfer coefficient within erosion disc, $W/(m^2 \cdot K)$
j	=	gas superficial velocity, m/s
k_j	=	thermal conductivity of impinging corium, W/(m•K)
M_c	=	cumulative concrete mass eroded, kg

$Nu = \frac{h_{conv} D_i}{k_i}$ = Nusselt number of impinging corium jet

P = ambient cavity pressure, Pa

Pr = Prandtl number of impinging corium jet

Q_i = mean forced convection heat flux within erosion disc, W/m^2

Re = Reynolds number of impinging corium jet

S = Stefan-Boltzmann constant, $W/(m^2 \cdot K^4)$

T_b = temperature of corium jet exiting breach, K

$T_{c,melt}$ = concrete melting temperature, K

T_i = temperature of corium jet impinging upon concrete, K

T_{int} = temperature at corium-slag film interface, K

$T_{oxide,freeze}$ = corium oxide phase freezing temperature, K

t = time, s

U_b = velocity of corium exiting breach, m/s

U_i = velocity of corium impinging upon concrete, m/s

Δe_c = concrete specific enthalpy change between initial temperature and liquidus temperature, J/kg

$\Delta\rho$ = $\rho_i - \rho_g$ = corium-gas density difference, kg/m^3

ε = corium emissivity

ρ_i = density of impinging corium, kg/m^3

ρ_g = density of gas rising through corium, kg/m^3

σ = corium-gas surface tension, N/m

ACKNOWLEDGEMENTS

This work was sponsored by the Electric Power Research Institute under Contract RP 2636-2. The authors gratefully appreciate the assistance of B. R. Sehgal, EPRI Project Manager. Figures were plotted by exchange student B. Artigny, CEA, Saclay. The manuscript was prepared by V. Eustace.

REFERENCES

1. J. J. Sienicki and B. W. Spencer, "Superheat Effects on Localized Vessel Breach Enlargement During Corium Ejection," Trans. Am. Nucl. Soc., 52, 1986, p. 522.

2. H. Martin, "Heat and Mass Transfer between Impinging Gas Jets and Solid Surfaces," Advances in Heat Transfer, Vol. 13, ed. J. P. Hartnett and T. F. Irvine, Jr., Academic Press, Inc., New York, 1977.

3. "Estimates of Early Containment Loads from Core Melt Accidents," NUREG-1079, U.S. Nuclear Regulatory Commission, December 1985, p. 2-7.

4. R. K. Cole, Jr., D. P. Kelly, and M. A. Ellis, "CORCON-Mod2: A Computer Program for Analysis of Molten-Core Concrete Interactions," NUREG/CR-3920, SAND84-1246, Sandia National Laboratories, August 1984.

5. I. Kataoka and M. Ishii, "Mechanistic Modeling and Correlations for Pool Entrainment Phenomena," NUREG/CR-3304, ANL-83-37, Argonne National Laboratory, April 1983.

6. J. C. M. Leung, G. A. Lambert, and L. J. Stachyra, "Transition to Dispersed Flow in a Stagnant Pool with Gas Injection," Trans. Am. Nucl. Soc., 38, 1981, p. 397.

7. I. Kataoka and M. Ishii, "Prediction of Pool Void Fraction by New Drift Flux Correlation," NUREG/CR-4657, ANL-86-29, Argonne National Laboratory, June 1986.

8. S. S. Kutateladze and I. G. Malenkov, "Boiling and Bubbling Heat Transfer under the Conditions of Free and Forced Convection," Heat Transfer 1978, Hemisphere Publishing Corporation, Washington, D.C., 1978, Vol. 1, p. 281.

9. "Effects of a Hypothetical Core Melt Accident on a PWR Vessel with Top-Entry Instruments," IDCOR Technical Report 15.2A, Atomic Industrial Forum, June 1983.

LIST OF FIGURES

15. Gas Superficial Velocity versus Time for Impingement of 86400 kg of Corium with 157 K of Superheat upon Basaltic Aggregate Concrete at Cavity Pressure of 0.4 MPa.

16. Concrete Mass Ablated versus Time for Impingement of 86400 kg of Corium with 157 K of Superheat upon Basaltic Aggregate Concrete.

17. Dependency of Total Concrete Mass Ablated upon Initial Corium Superheat for Impingement of 86400 kg of Corium with 157 K of Superheat upon Limestone Aggregate-Common Sand Concrete.

18. Dependency of Corium Incremental and Total Bulk Temperature Reductions upon Initial Corium Superheat for Impingement of 86400 kg of Corium with 157 K of Superheat upon Basaltic Aggregate Concrete Assuming Presence of Oxide Crust and Concrete Slag Film.

19. Dependency of Corium Incremental and Total Bulk Temperature Reductions upon Initial Corium Superheat for Impingement of 86400 kg of Corium with 157 K of Superheat upon Basaltic Aggregate Concrete Assuming Presence of Concrete Slag Film without Oxide Crust Formation.

20. Dependency of Corium Incremental and Total Bulk Temperature Reductions upon Initial Corium Superheat for Impingement of 86400 kg of Corium with 157 K of Superheat upon Basaltic Aggregate Concrete Assuming Presence of Oxide Crust without Concrete Slag Film.

21. Dependency of Corium Total Bulk Temperature Reduction upon Initial Corium Superheat for Impingement of 86400 kg of Corium upon Basaltic Aggregate Concrete.

22. Dependency of Corium Total Bulk Temperature Reduction upon Impinging Corium Mass for Impingement of Corium with 157 K of Superheat upon Basaltic Aggregate Concrete.

23. Dependency of Corium Total Bulk Temperature Reduction upon Initial Breach Diameter for Impingement of Corium with 157 K of Superheat upon Limestone Aggregate-Common Sand Concrete.

~~LIMESTONE CONCRETE~~

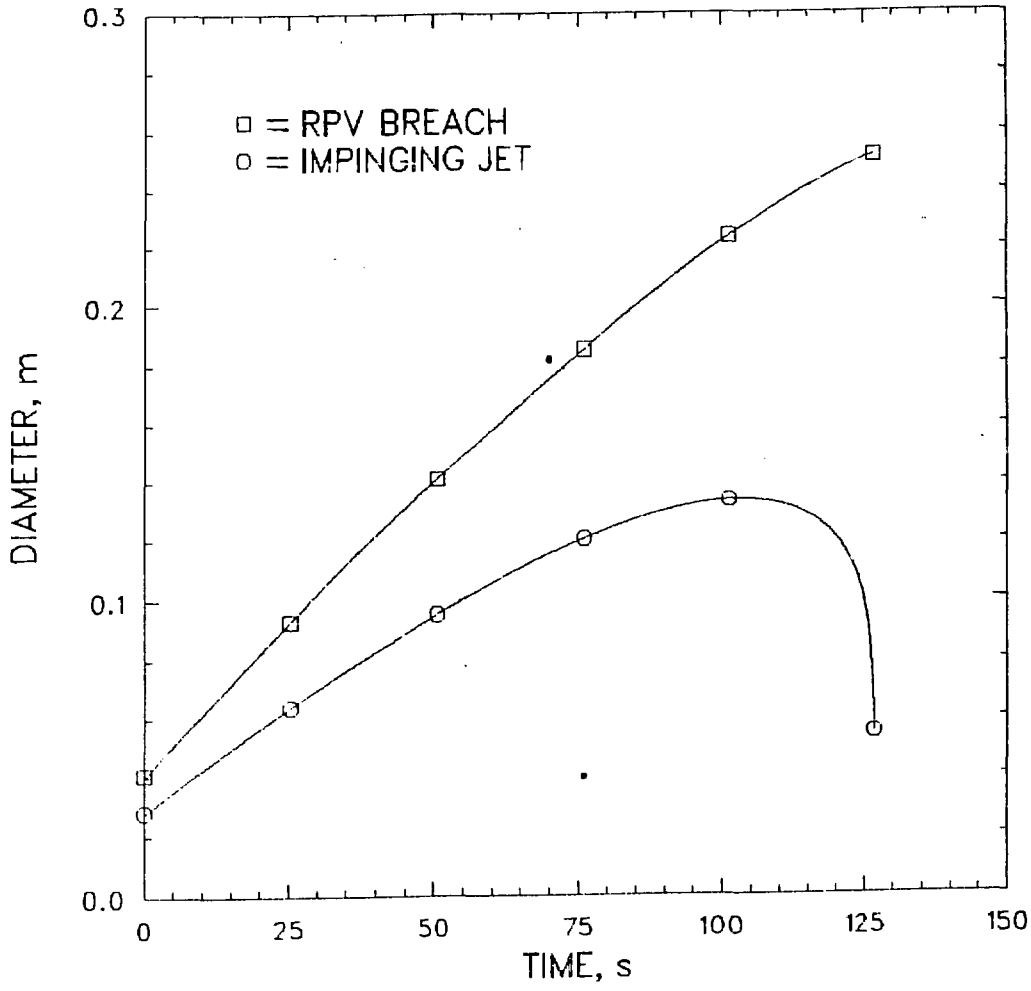

Fig 1
Dave

F36496

T3DB3

NORMAL TERMINATION

AUG 6, 1986 SPVERSI: V=1.2

9:30 AM IES NUMBER=9977

~~LIMESTONE CONCRETE~~

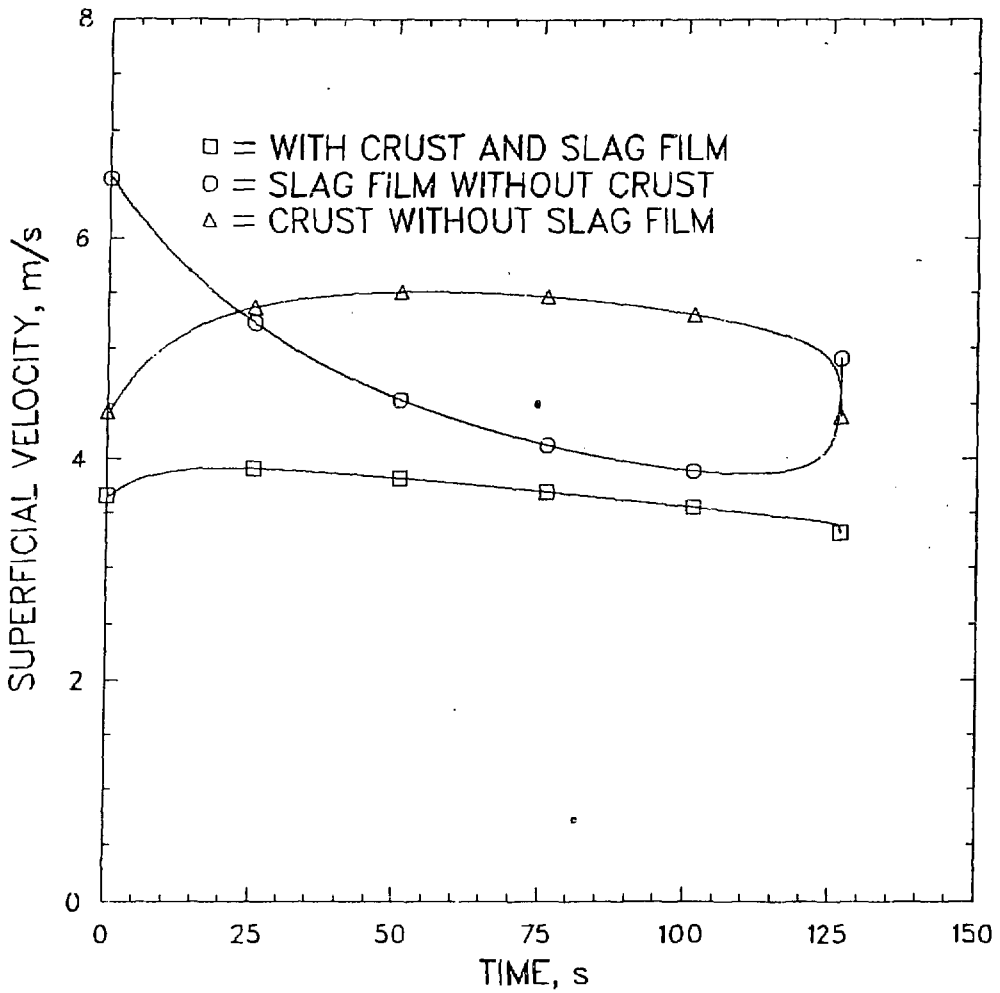

Fig 2
0.1 MPa
Save

F36496
T3UGSUPL
NORMAL TERMINATION
AUG 7, 1986 SPVERSII V=1.2
2:24 PM JES NUMBER-7085

~~LIMESTONE CONCRETE~~

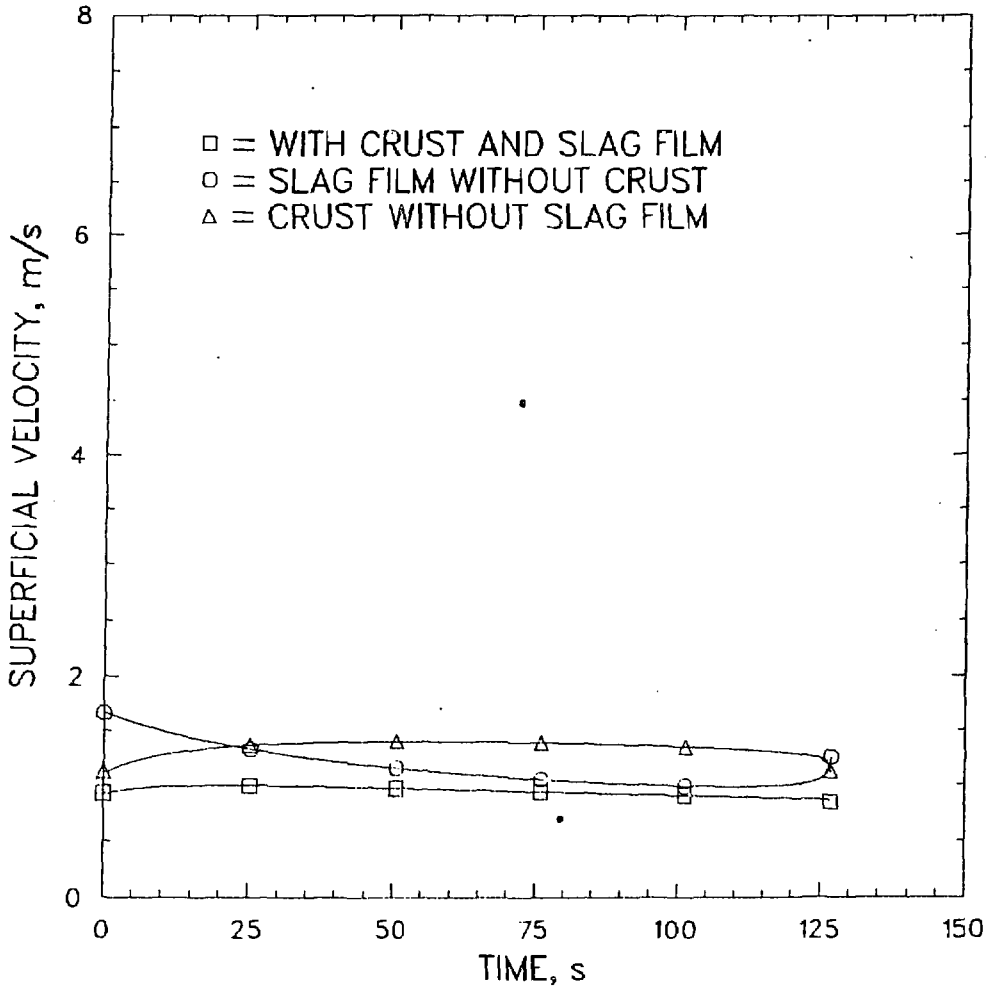

0.4 MPa

Save

F36496

T3UGSUPL

NORMAL TERMINATION

AUG 6, 1996 SPVERS11 V=1.2

9:16 AM JES NUMBER-9869

~~LIMESTONE CONCRETE~~

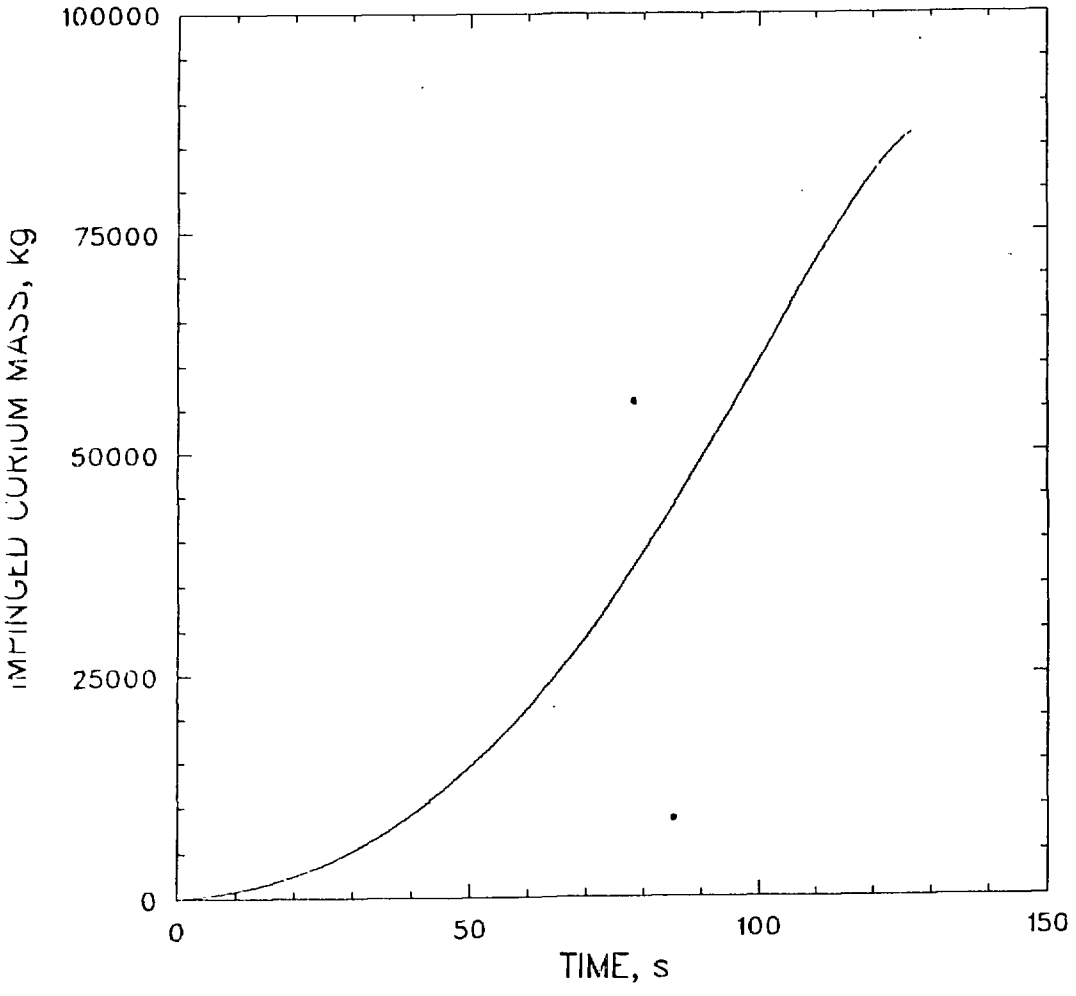

Fig. 4
Dave

F36496

TFMINJL

NORMAL TERMINATION

AUG 7, 1986 SPVERSII V=1.2

2:29 PM JES NUMBER-7091

~~LIMESTONE CONCRETE~~

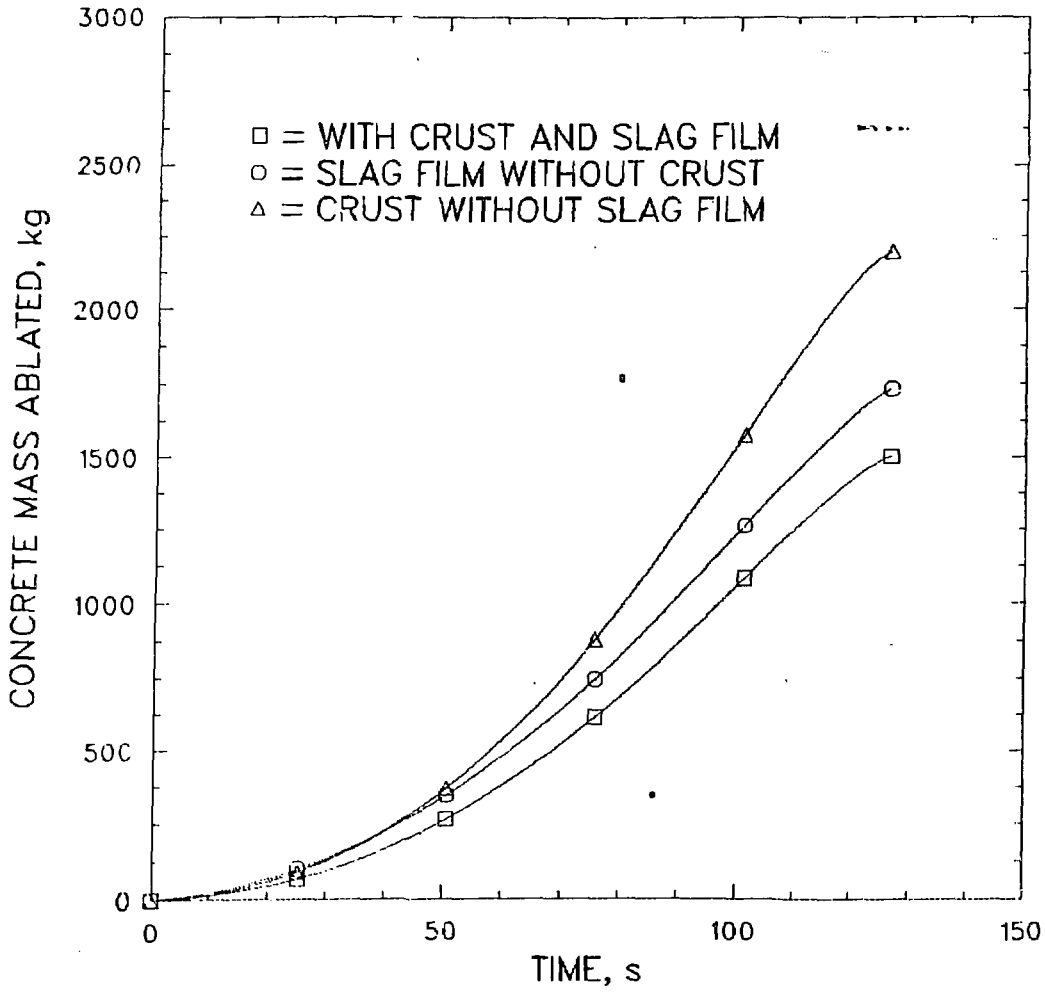

F36496

TFMCL

NORMAL TERMINATION

AUG 6, 1986 SPVERS11 V=1.2

1:26 PM JES NUMBER=173

~~EFFECTS OF CORIUM SUPERHEAT UPON IMPINGEMENT TIME~~

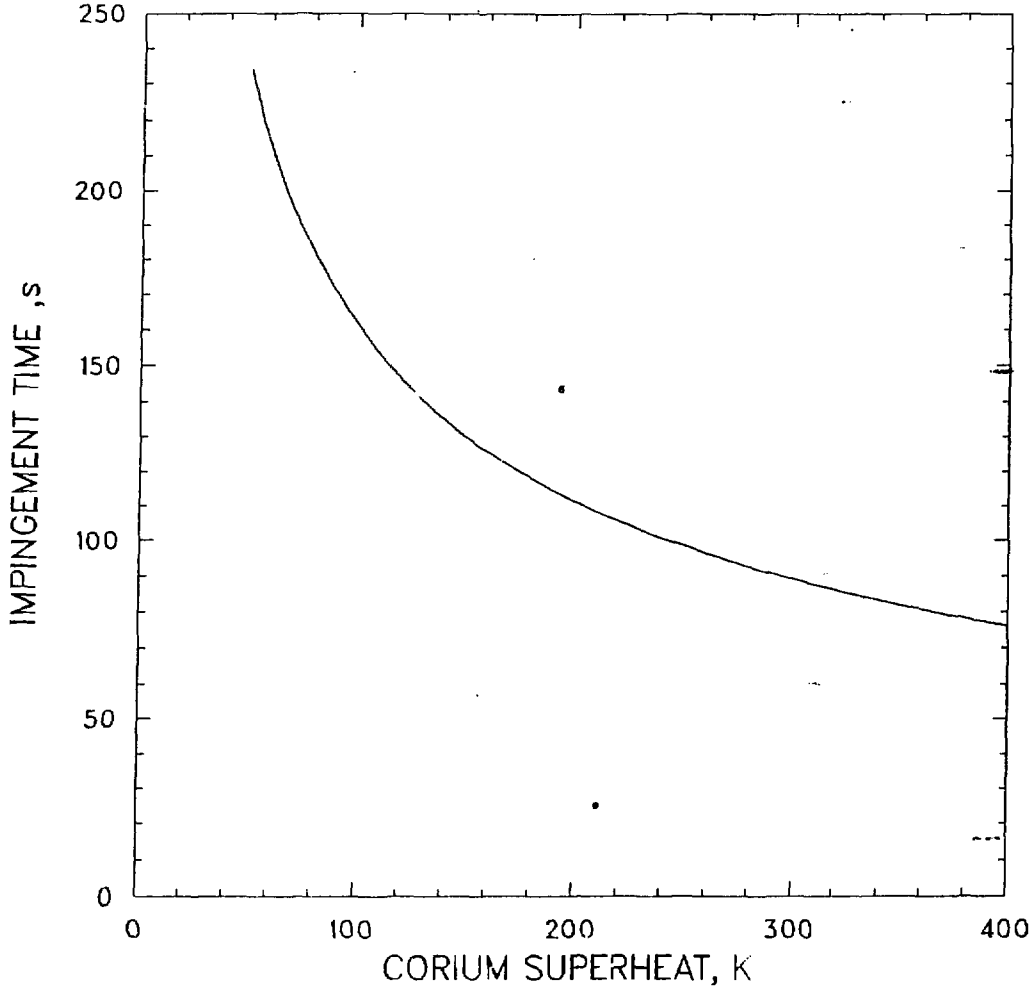

Fig. 6
Save

F36496
EJECTIME
NORMAL TERMINATION
AUG 7, 1986 SPVERS11 V=1.2
2:58 PM JES NUMBER-7099

~~LIMESTONE CONCRETE~~

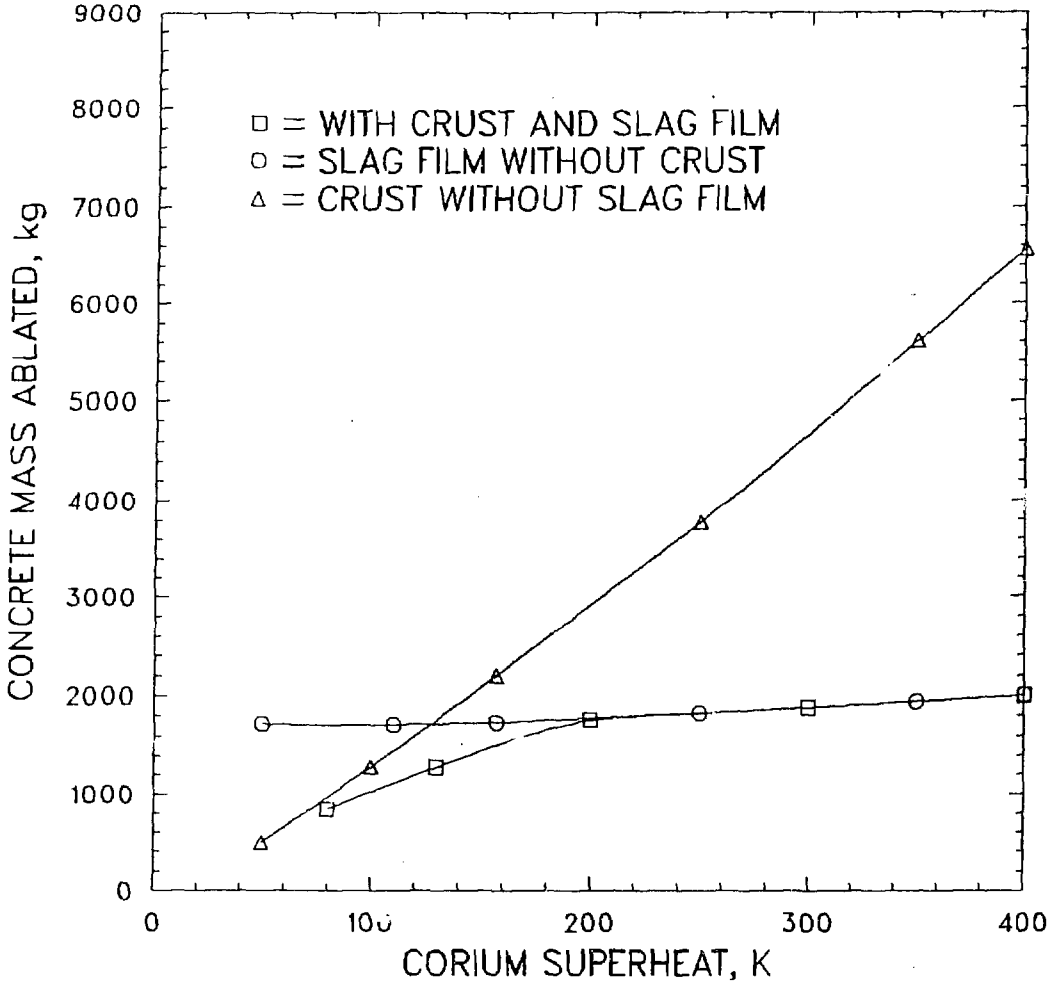

~~Fig~~ 7 Fig

have

F36496

LABLS2

NORMAL TERMINATION

AUG 18, 1986 SPVERS11 V-1.3

9:43 AM JES NUMBER-96E

~~LIMESTONE CONCRETE~~

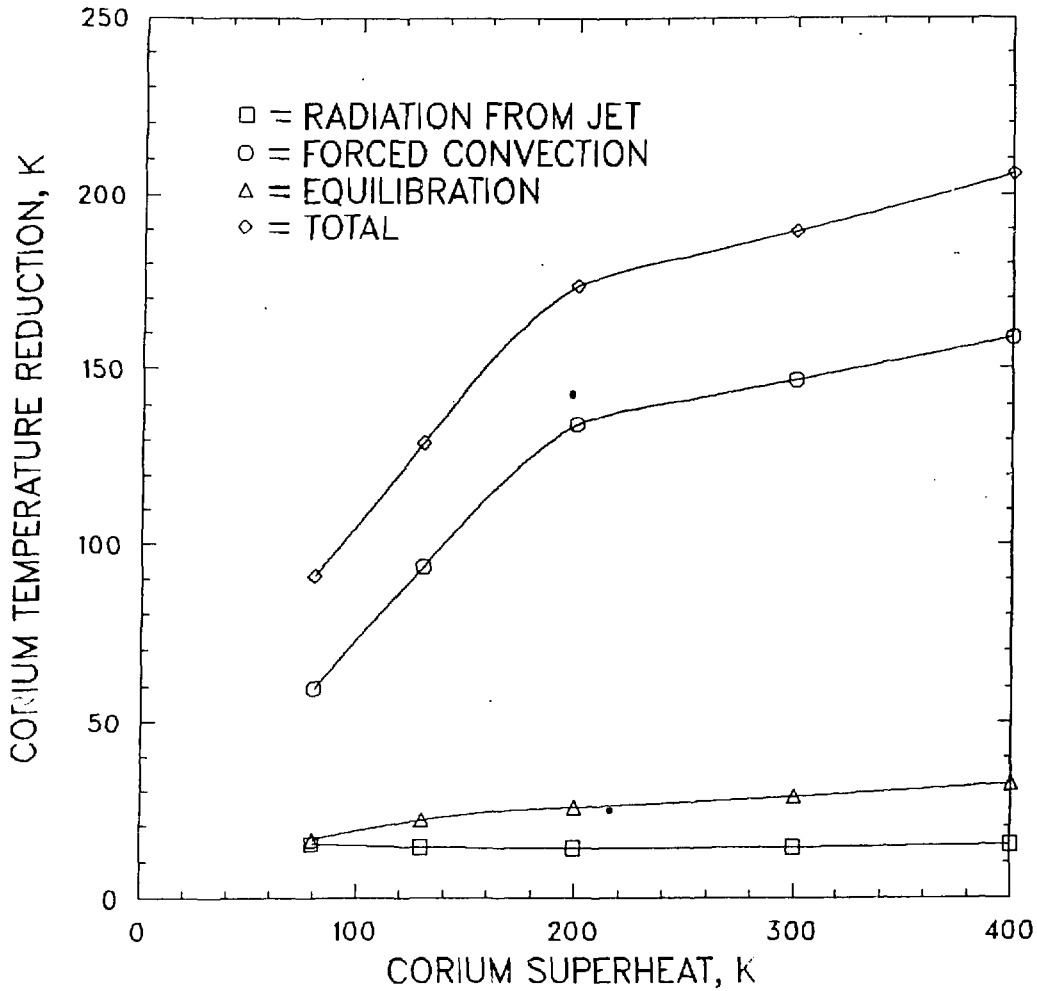

Fig. 8

F36496
LABL1
NORMAL TERMINATION
AUG 4, 1986 SPVERS11 V=1.2
11:02 AM JES NUMBER-1091

~~LIMESTONE CONCRETE~~

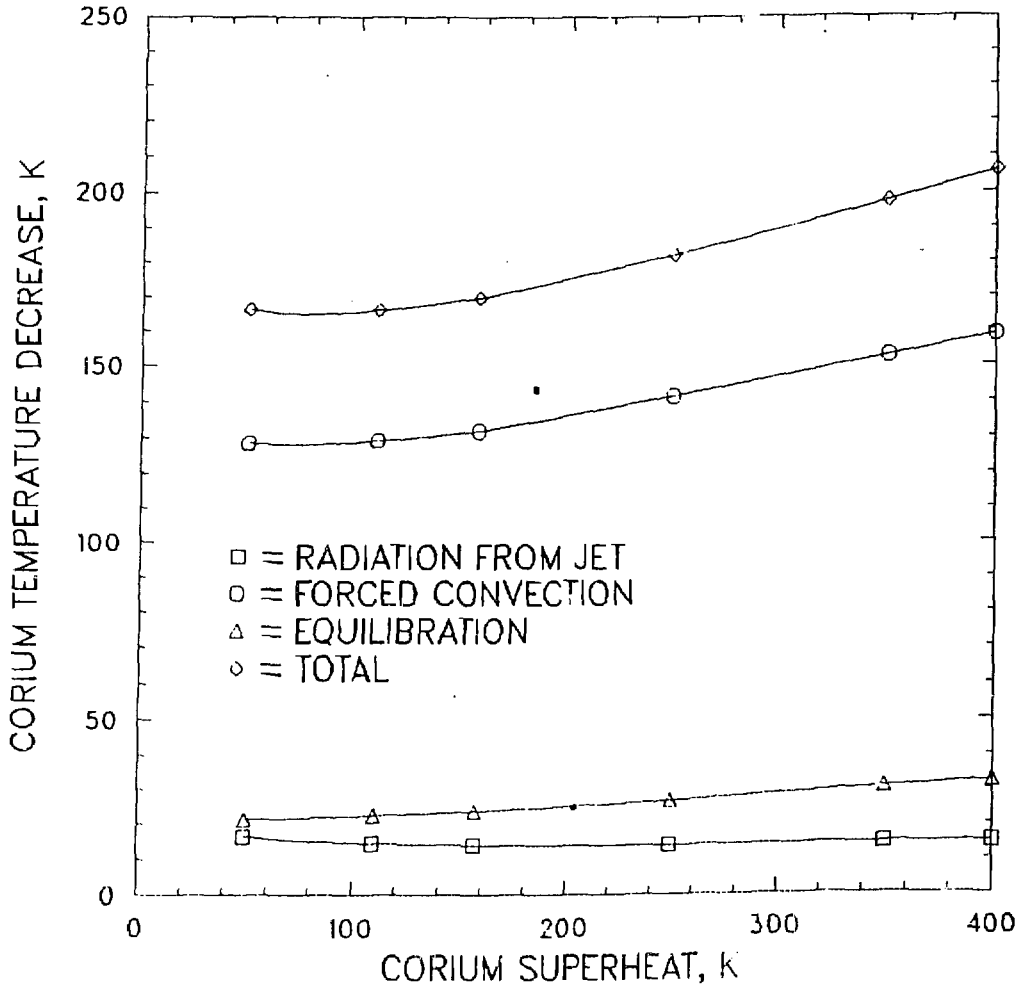

Fig. 7
T. Lowe

F36496
LABL2

NORMAL TERMINATION

AUG 5, 1986 SPVERSII V=1.2

2:47 PM JES NUMBER=7386

~~LIMESTONE CONCRETE~~

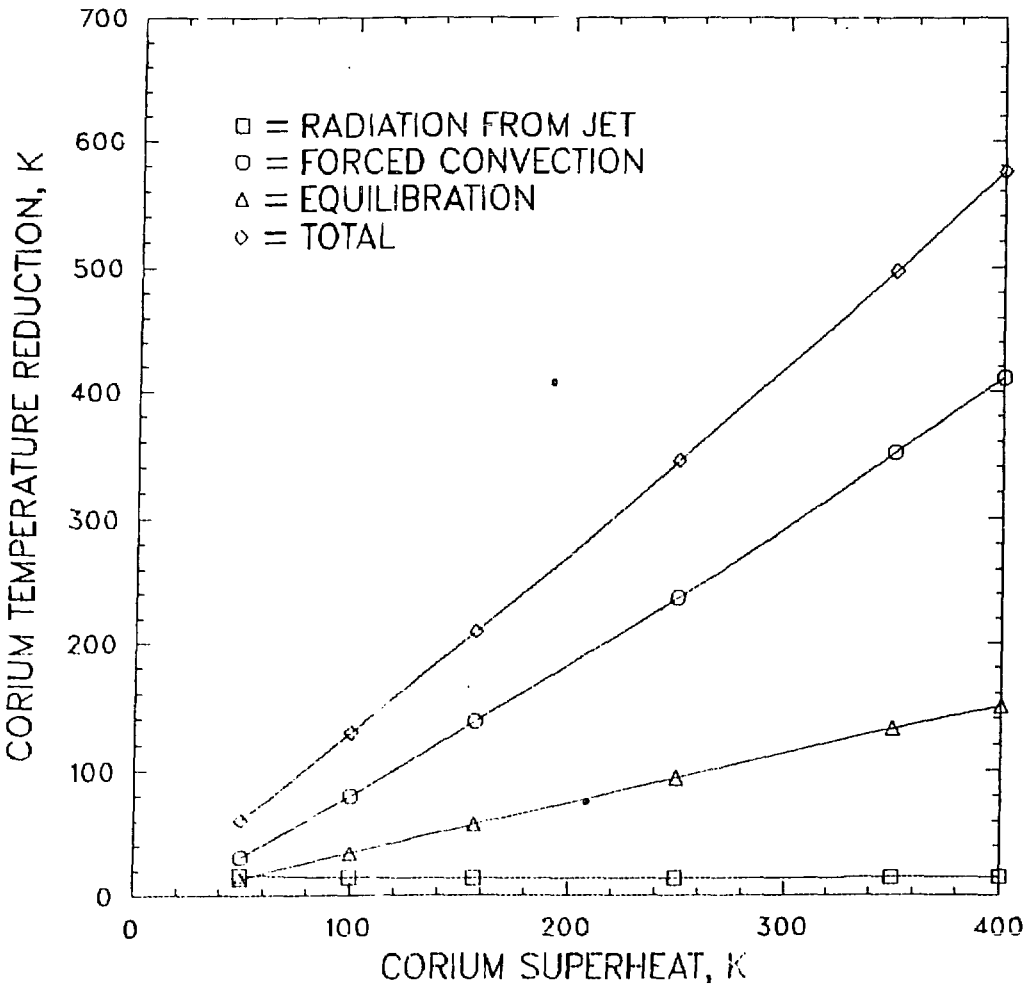

fig 10

F36496

LABL5

NORMAL TERMINATION

AUG 6, 1986 SPVERSII V=1.2

1:25 PM JES NUMBER=1719

~~LIMESTONE CONCRETE~~

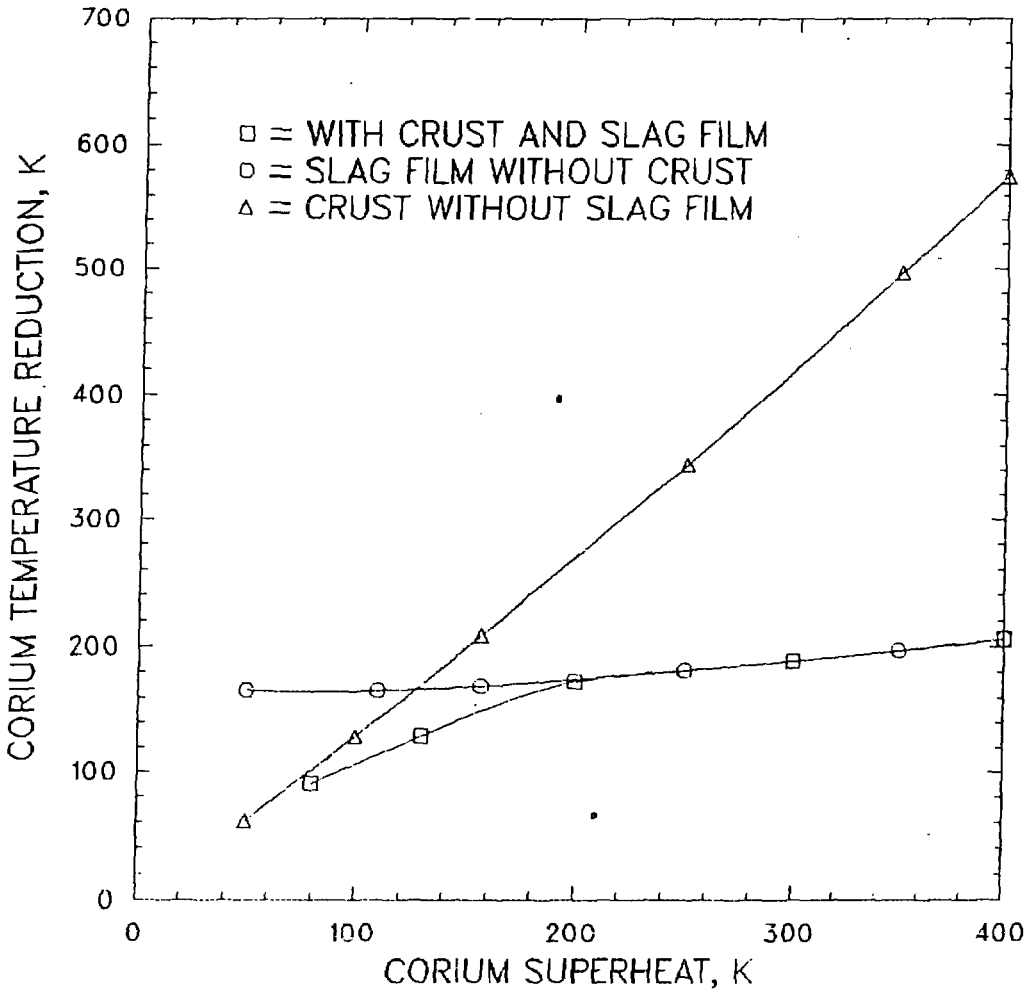

Fig 11

F36496

LABLS

NORMAL TERMINATION

AUG 6, 1986 SPVERSII V=1.2

1:49 PM JES NUMBER-1856

~~LIMESTONE CONCRETE~~

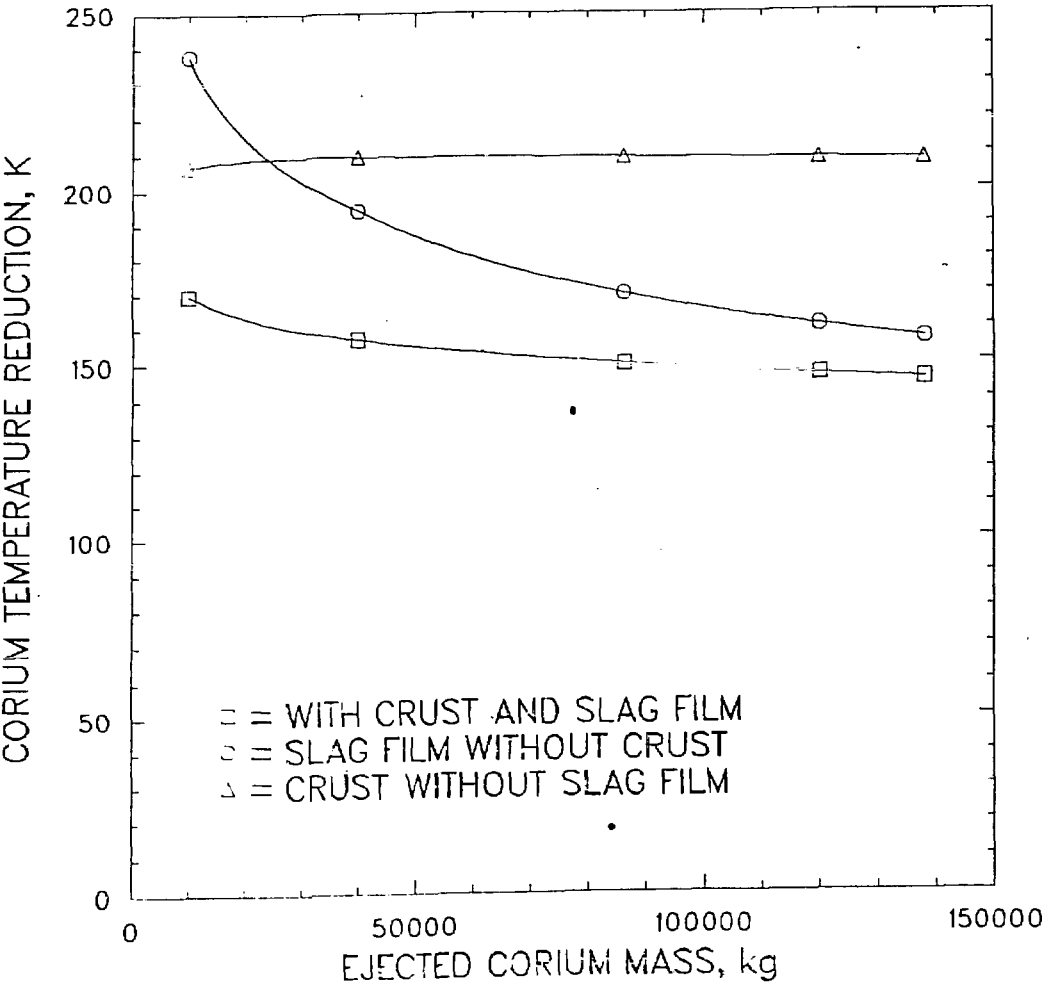

Fig 12
Rev

F36496

EJECTL

NORMAL TERMINATION

AUG 5, 1986 SPVERSII V=1.2

10:31 AM JES NUMBER-5655

~~LIMESTONE CONCRETE~~

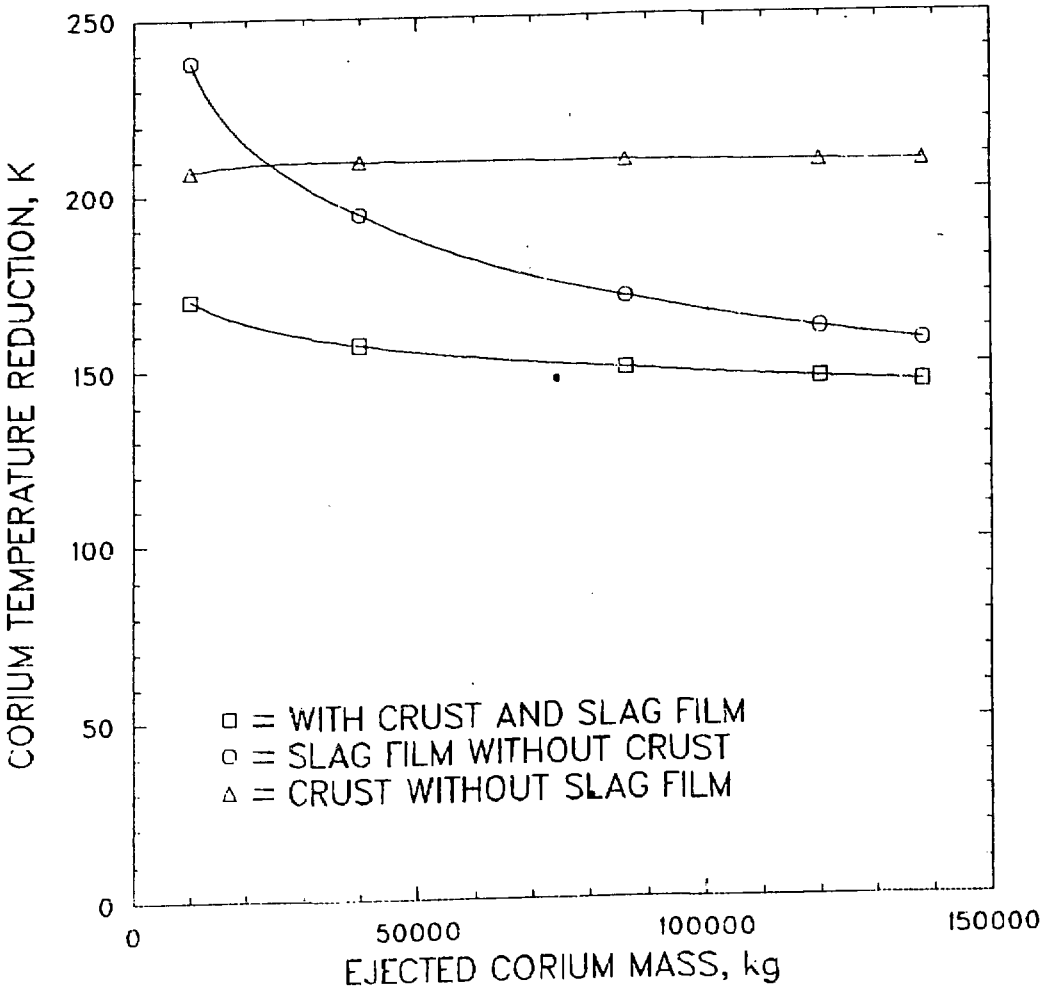

Eq. 12
Lit

F36496

EJECTL

NORMAL TERMINATION

AUG 5, 1986 SPVERSII V=1.2

2:48 PM JES NUMBER-7394

~~LIMESTONE CONCRETE~~

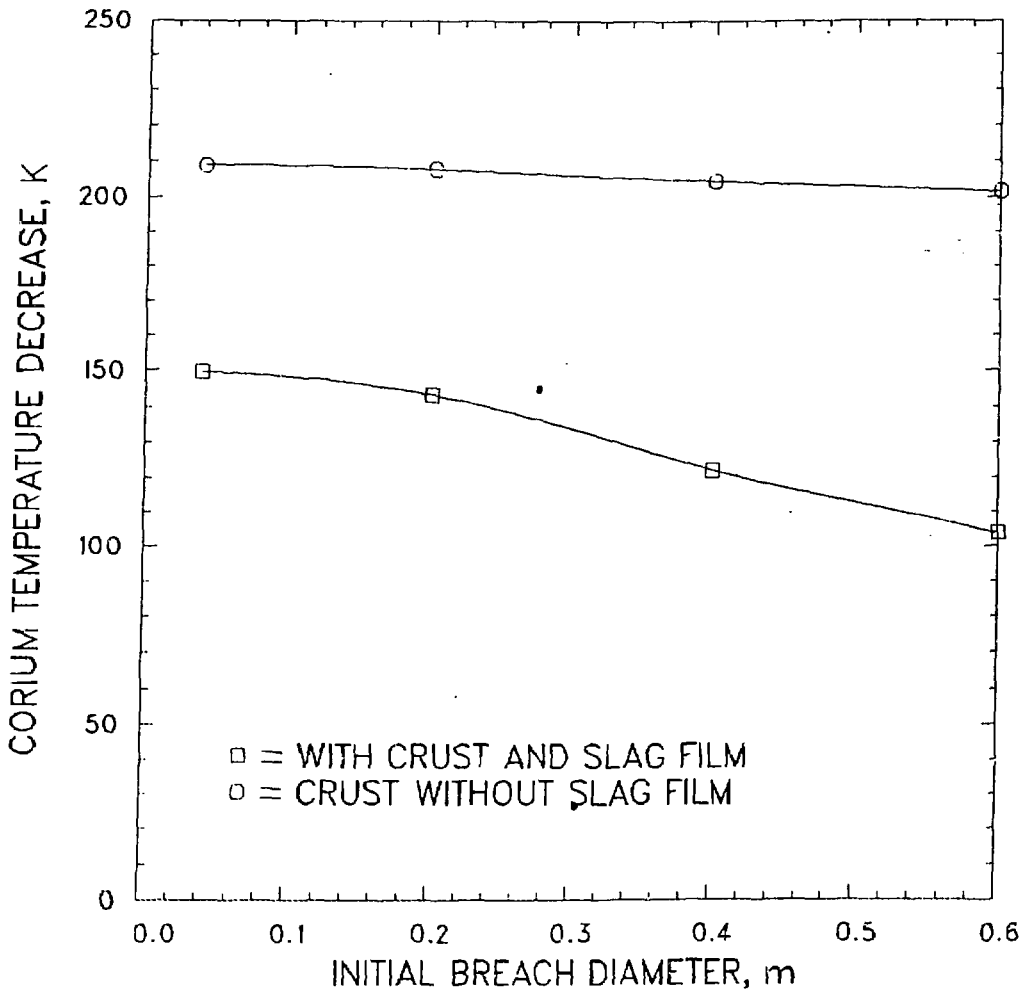

Fig. 13

F36496

TDBOL

NORMAL TERMINATION

AUG 5, 1986 SPVCRS11 V=1.2

2:43 PM JES NUMBER=7343

~~BASALT CONCRETE~~

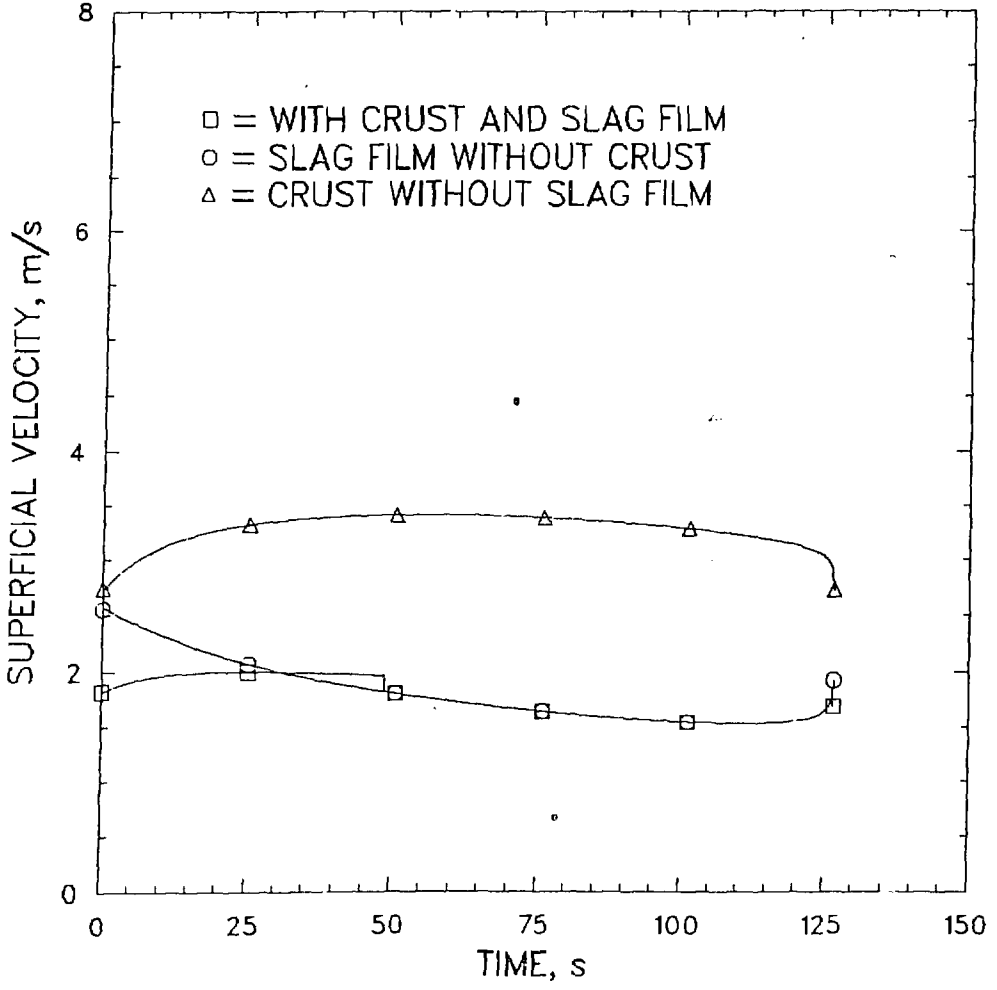

Fig. 14
0.1 MPa
Dave

F36496
T3UGSUPB
NORMAL TERMINATION
AUG 7, 1986 SPVERS11 V=1.2
3:01 PM JES NUMBER-7111

~~BASALT CONCRETE~~

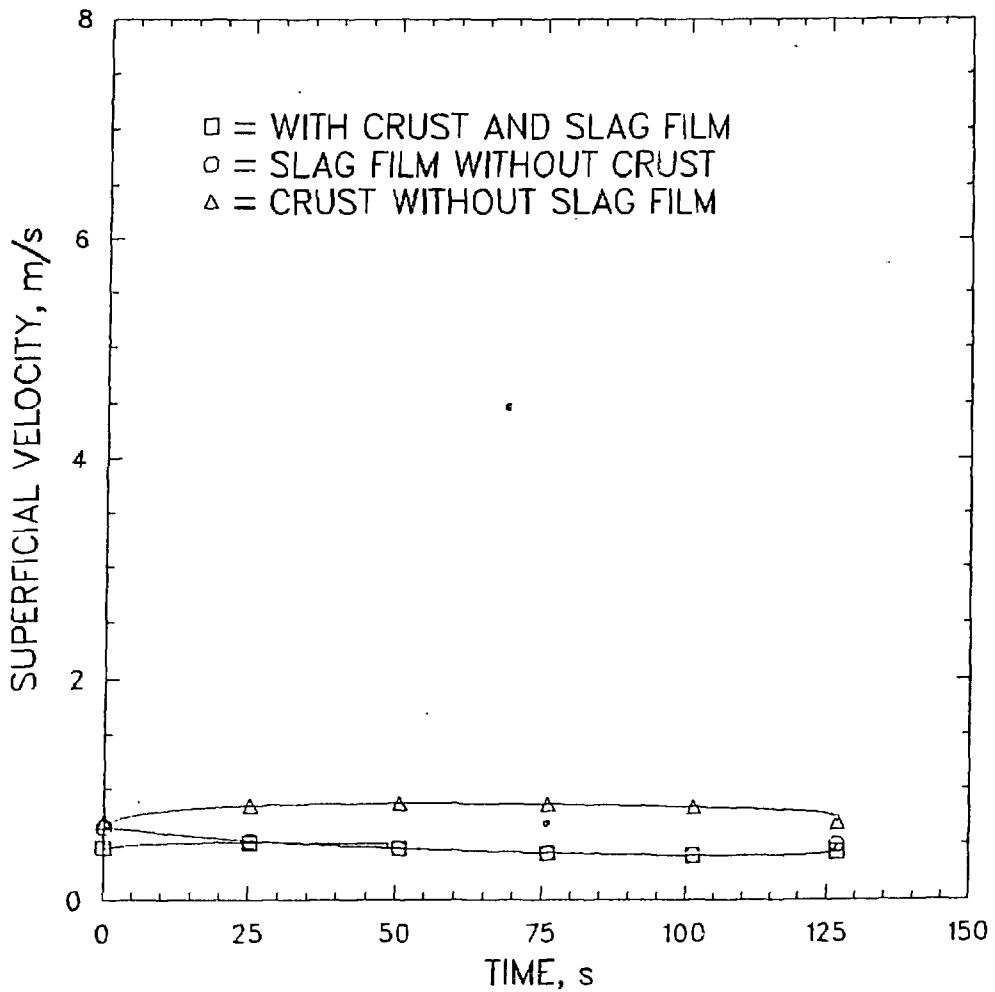

Fig 15
0.4 MPa
Save

F36496

T3UGSUPB

NORMAL TERMINATION

AUG 7, 1986 SPVERSII V=1.2

3:16 PM JES NUMBER-7121

~~BASALT CONCRETE~~

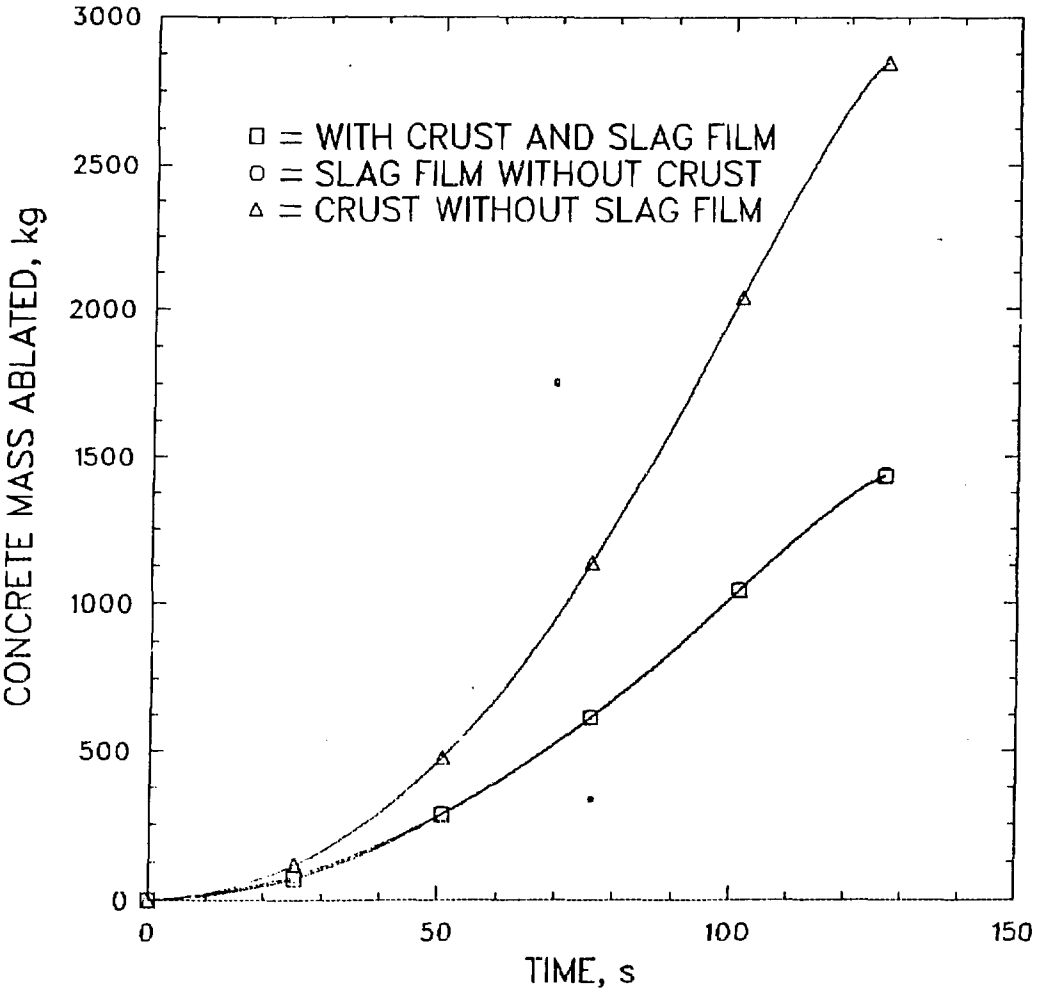

F36496

TFMCB

NORMAL TERMINATION

AUG 6, 1986 SPVERSI1 V=1.2

~~BASALT CONCRETE~~

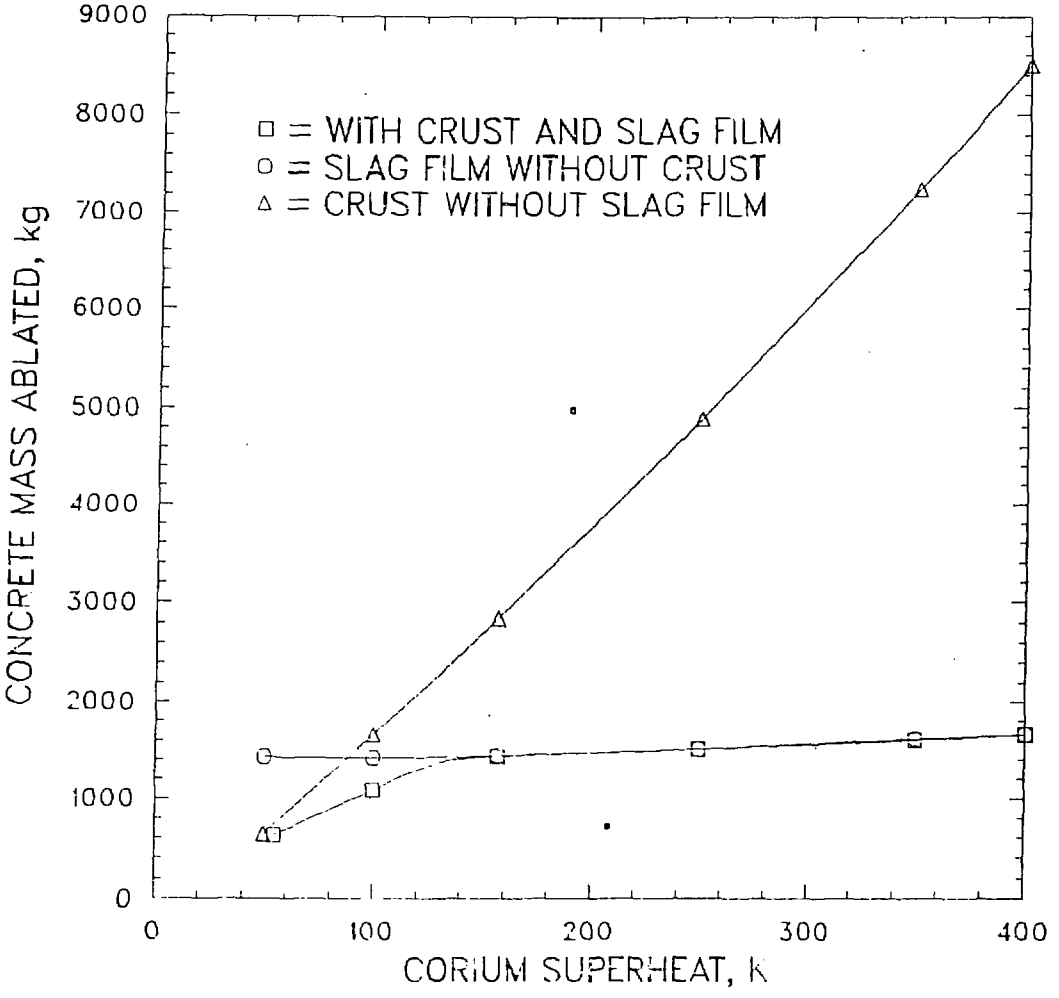

F36496

BABLS2

NORMAL TERMINATION

AUG 11, 1996 SPVERSII V=1.2

9:33 AM JES NUMBER-5179

~~BASALT CONCRETE~~

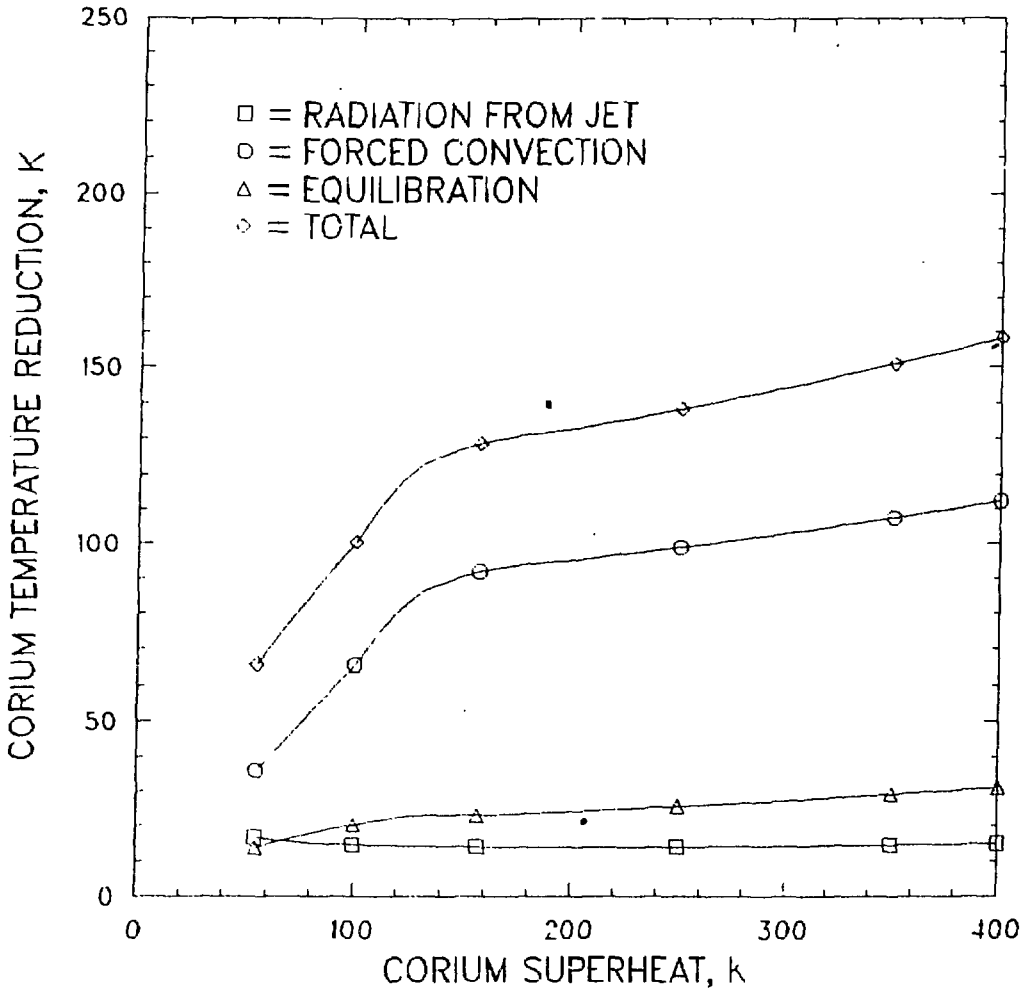

F36496

BABL1

NORMAL TERMINATION

AUG 5, 1986 SPVERSII V=1.2

4:55 PM JES NUMBER=8310

~~BASALT CONCRETE~~

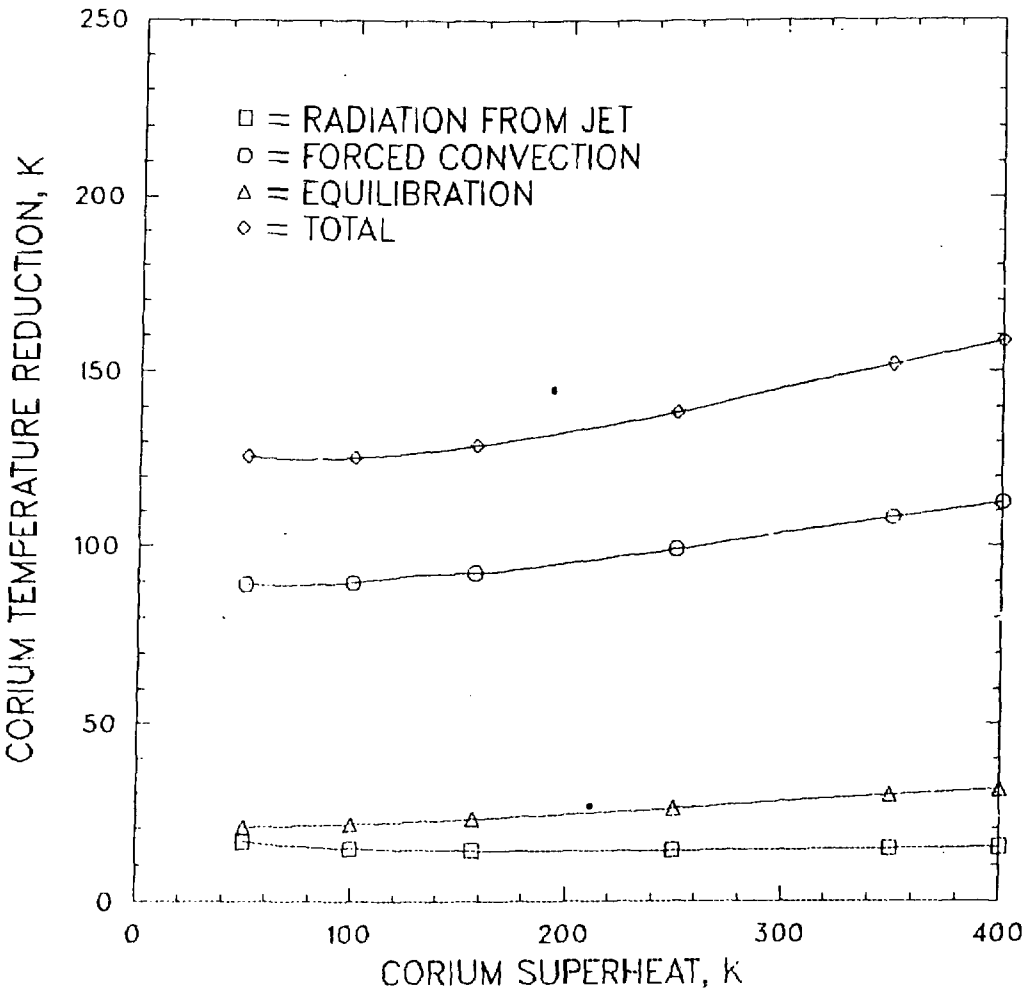

F36496

BABL2

NORMAL TERMINATION

AUG 6, 1986 SPVERSII V=1.2

1-24 PM JES NUMBER=1710

~~BASALT CONCRETE~~

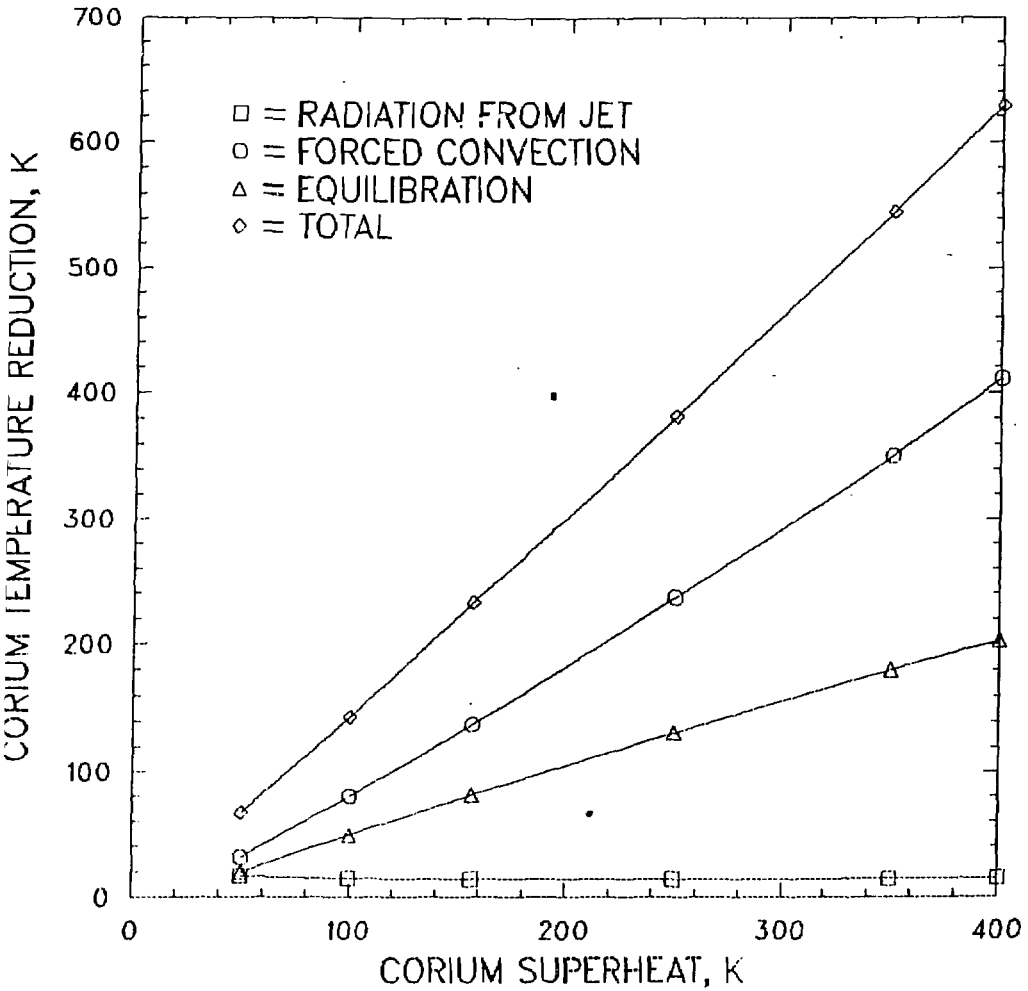

Fig. 20
Save

F36496
BABL5

NORMAL TERMINATION
AUG 6, 1986 SPVERS11 V=1.2
10:57 AM JES NUMBER=0873

~~BASALT CONCRETE~~

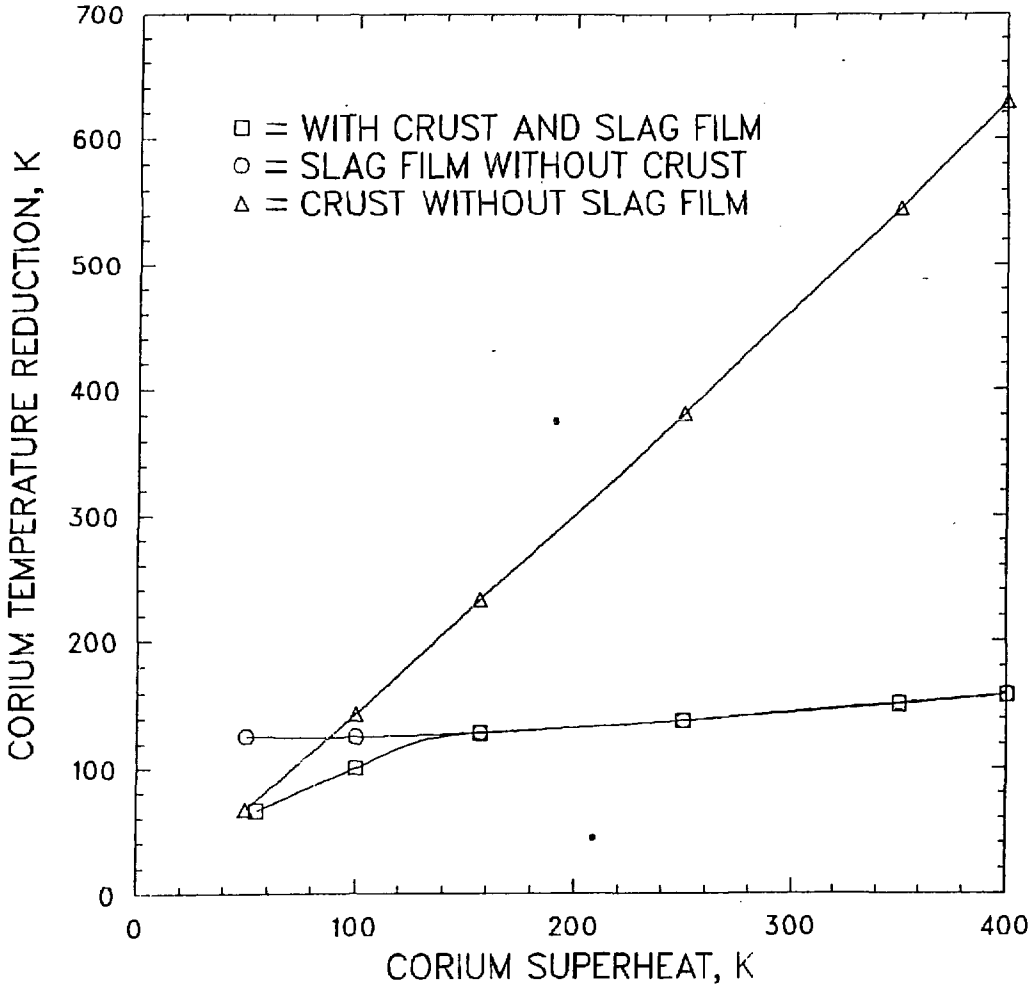

Fig. 21
Dave

F36496
BABLS

NORMAL TERMINATION
AUG 7, 1986 SPVERS11 V=1.2
3:01 PM JES NUMBER-7123

~~BASALT CONCRETE~~

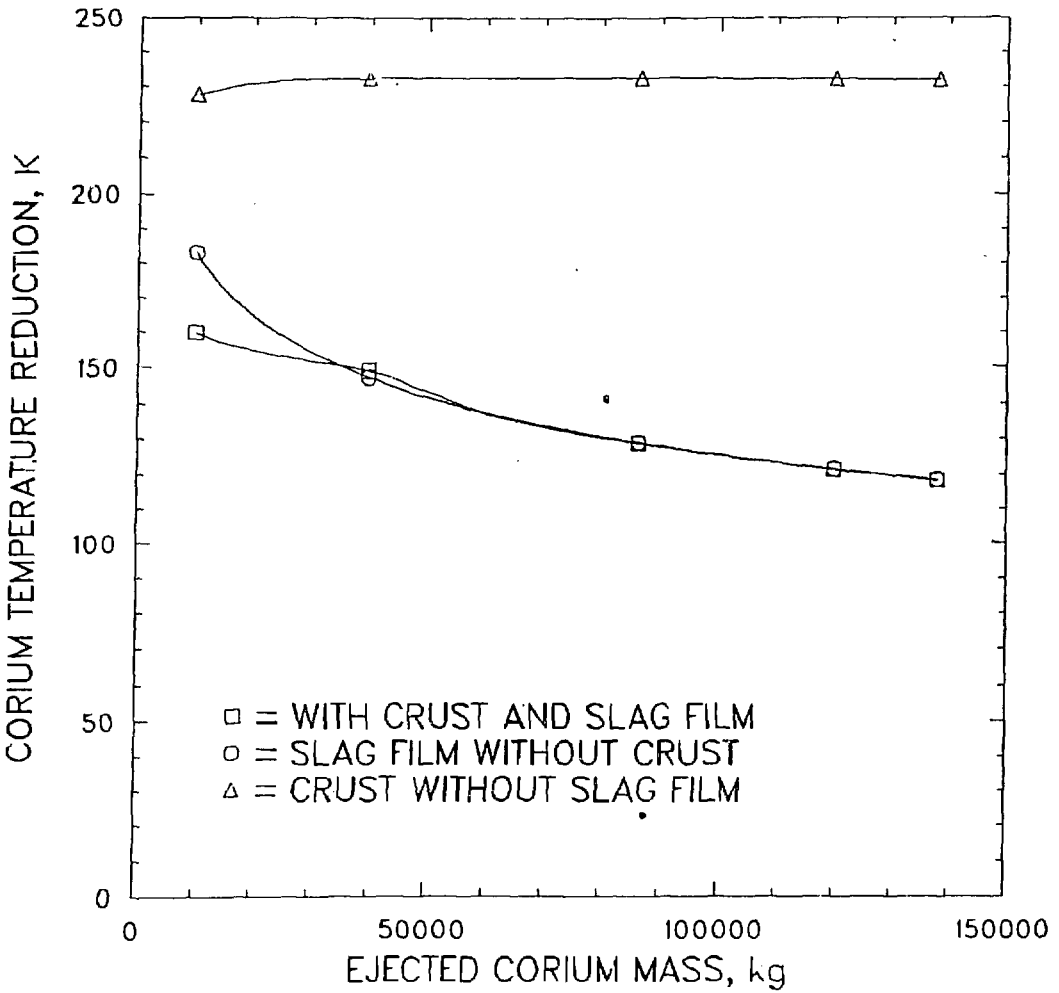

Fig. 22
Save

F36496
EJECTB
NORMAL TERMINATION
AUG 7, 1986 SPVERS11 V=1.2
3:01 PM JES NUMBER-7124

~~BASALT CONCRETE~~

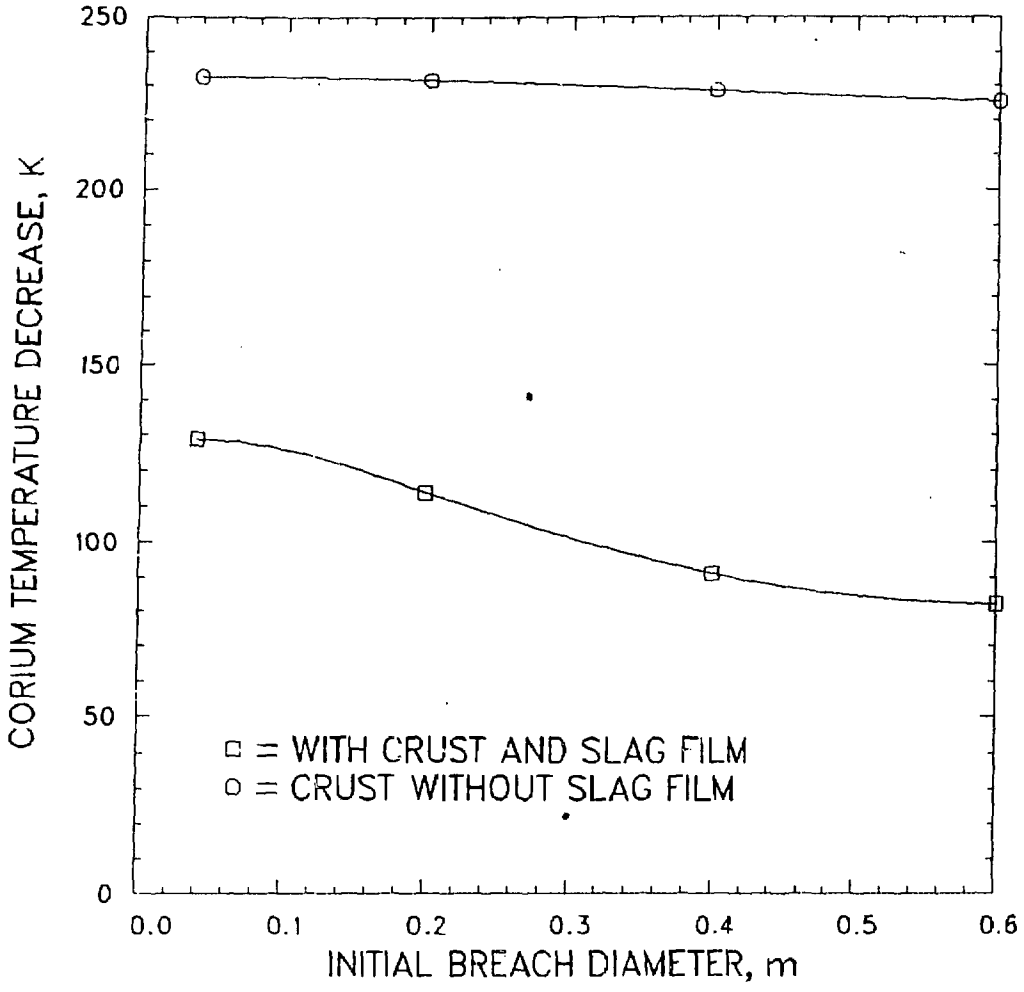

12 aug. 23

F36496

TDBOB

NORMAL TERMINATION

AUG 5, 1996 SPVERSII V=1.2

2:41 PM JES NUMBER-7331